

# **Zooming into the Inner Helmholtz Plane of Pt(111)-Aqueous Solution Interfaces: Chemisorbed Water and Partially-Charged Ions**

Jun Huang

Institute of Energy and Climate Research, IEK-13: Theory and Computation of Energy Materials,  
Forschungszentrum Jülich GmbH, 52425 Jülich, Germany

Email: [ju.huang@fz-juelich.de](mailto:ju.huang@fz-juelich.de)

## **Abstract**

The double layer on transition metals, i.e., platinum, features chemical metal-solvent interactions and partially charged chemisorbed ions. Chemically adsorbed solvent molecules and ions are situated closer to the metal surface than electrostatically adsorbed ions. This effect is described tersely by the concept of an inner Helmholtz plane (IHP) in classical double layer models. The IHP concept is extended here in three aspects. Firstly, a refined statistical treatment of solvent (water) molecules considers a continuous spectrum of orientational polarizable states, rather than a few representative states, and non-electrostatic, chemical metal-solvent interactions. Secondly, chemisorbed ions are partially charged, rather than being electroneutral, with the coverage determined by a generalized, energetically-distributed adsorption isotherm. The surface dipole moment induced by partially-charged, chemisorbed ions is considered. Thirdly, considering different locations and properties of chemisorbed ions and solvent molecules, the IHP is divided into two planes, namely, an AIP (adsorbed ion plane) and ASP (adsorbed solvent plane). The model is used to study how the partially-charged AIP and polarizable ASP lead to intriguing double-layer capacitance curves that are different from what conventional Gouy-Chapman-Stern model describes. The model provides an alternative interpretation for recent capacitance data of Pt(111)-aqueous solution interfaces calculated from cyclic voltammetry (CV). The implications, limitations, and experimental confirmation of the present model are discussed.

## **Introduction**

There is a wave of renewed interest in the electric double layer (EDL) structure in electrocatalysis, probably due to two reasons.<sup>1-4</sup> On the one hand, the activity of many electrocatalytic reactions is revealed to be affected markedly by electrolyte cations<sup>5-9</sup> and pH<sup>10-13</sup>. There is growing consensus that demystifying these electrolyte effects requires fundamental knowledge of the EDL,<sup>3, 14</sup> as discussed in several review articles.<sup>14-17</sup> On the other hand, a growing body of experimental data on the EDL of single crystals of transition metals, notably platinum, have been reported recently.<sup>4, 18-23</sup> These new data, though not fully consistent as detailed below, have already surprised us as they do not agree, even qualitatively, with classical double layer models.

A well-documented classical model is the Gouy-Chapman-Stern (GCS) model, which describes the EDL as a series combination of an inner layer and a diffuse layer.<sup>24</sup> The GCS model has many variants, with detailed treatments of the diffuse layer and the inner layer.<sup>25-27</sup> A hallmark of GCS-like models is the appearance of a minimum in the differential double-layer capacitance ( $C_{dl}$ ) curve, named the Gouy-Chapman minimum, at a particular electrode potential, named the potential of zero charge (pzc), in dilute electrolyte solutions. Moving away from the pzc in cathodic and anodic directions,  $C_{dl}$  grows and then decreases, resulting in a camel-shaped  $C_{dl}$  profile with two peaks and one valley. The two peaks usually signify overcrowding of counterions near the metal surface, which are usually asymmetric due to different sizes of cations and anions. The two peaks move closer and eventually melt into a single peak as the electrolyte solution gets more and more concentrated.<sup>28, 29</sup>

The aptness of the GCS model has been corroborated on mercury-like electrodes, firstly by Gouy in the 1910s,<sup>30</sup> and then by Grahame in the 1940s and 1950s,<sup>31</sup> e.g., see Parsons's review.<sup>32</sup> In the presence of specific adsorption of anions, Grahame discriminated an inner Helmholtz plane (IHP) and an outer Helmholtz plane (OHP) in the inner layer.<sup>31</sup> More than just a refinement of the Stern model, the Grahame model sowed the seeds of subsequent developments in the EDL theory, including the consideration of field-dependent orientation of water molecules,<sup>33-36</sup> discreteness of adsorbed ions,<sup>37-40</sup> and quantum effects of metal electrons,<sup>41-44</sup> as discussed in a recent tutorial.<sup>27</sup> Valette and Hamelin and coworkers have demonstrated that the GCS model is valid also for silver single crystals in nonspecifically adsorbing electrolytes.<sup>45-48</sup>

The idyll reaches an end for platinum. The Gouy-Chapman minimum is absent in the study of Pajkossy and Kolb where  $C_{dl}$  of Pt(111) in a  $KClO_4$  and  $HClO_4$  mixture electrolyte with a concentration down to 1 mM was measured.<sup>18, 20, 49</sup> Instead, their data show a  $C_{dl}$  peak near the pzc in the anodic direction. Contrarily, Xue et al. observed Gouy-Chapman minimums for Pt(111) in 0.05 M  $MeClO_4$  electrolytes ( $Me=Li, Na, K, Rb, Cs$ ), however, at potentials  $\sim 0.2$  V below the pzc.<sup>23</sup> More recently, Ojha et al. observed the Gouy-Chapman minimum for Pt(111) in 0.1 mM  $HClO_4$ .<sup>21, 22</sup> In addition, they found that the

Gouy-Chapman minimum turns into a maximum near the pzc when increasing the electrolyte solution above 1 mM, qualitatively consistent with previous observations of Pajkossy and Kolb.<sup>18, 20, 49</sup>

One should be aware of the discrepancy in the magnitude of  $C_{dl}$  of Pt(111) at the pzc, denoted  $C_{dl,pzc}$ , in different studies.  $C_{dl,pzc}$  is around  $20 \mu F cm^{-2}$  in the study of Pajkossy and Kolb using an electrolyte concentration of 0.1 M,<sup>18, 20, 49</sup> in the range of  $10\text{--}30 \mu F cm^{-2}$  for 0.05 M NaOH and 0.10 M HClO<sub>4</sub> in the study of Schouten, van der Niet and Koper,<sup>50</sup> around  $30 \mu F cm^{-2}$  in the study of Xue et al. with an electrolyte concentration of 0.05 M,<sup>23</sup> and around  $100 \mu F cm^{-2}$  in the study of Ojha et al. with an electrolyte concentration of 0.005 M.<sup>21, 22</sup> Note that  $C_{dl,pzc}$  shall decrease with the electrolyte concentration, according to the GCS model. Surprisingly enough, recent values of  $C_{dl,pzc}$  in more dilute electrolyte solutions are even several folds higher than previous values in more concentrated electrolyte solutions. Understanding the origin of the anomalously large  $C_{dl,pzc}$  is an open question on which several viewpoints already exist, which I am about to discuss, and that motivates this study.

To rationalize the large  $C_{dl,pzc}$ , Doblhoff-Dier and Koper introduced weak (around several hundred meVs), attractive ion–surface interaction, of which possible origins are also discussed.<sup>51</sup> This effectively increases the ion concentration in the double layer, shortens the Debye length, and magnifies the magnitude of  $C_{dl,pzc}$ . Recently, Schmickler rationalized the higher  $C_{dl,pzc}$  as a consequence of weak specific adsorption of anions.<sup>52</sup> The introduction of anion adsorption can increase the overall capacitance, and decrease the Parsons-Zobel slope. However, this model cannot explain that the Parsons-Zobel slopes are not sensitive to the identity of electrolyte anions.<sup>22</sup> More recently, Ojha, Doblhoff-Dier and Koper modified their previous model by further adopting a two-state submodel for the first-layer water molecules,<sup>22</sup> which was developed earlier by Le et al.<sup>53</sup>

This marked and surprising discrepancy in  $C_{dl,pzc}$  might be ascribed to different methods used to determine  $C_{dl}$ . Pajkossy and Kolb extracted  $C_{dl}$  from electrochemical impedance spectroscopy (EIS) data using the Frumkin–Melik–Gaikazyan (FMG) model.<sup>18, 20, 49</sup> Xue et al. extracted  $C_{dl}$  from EIS data using an electric circuit model involving empirical constant phase elements.<sup>23</sup> Ojha et al. calculated  $C_{dl}$  from cyclic voltammogram (CV) data.<sup>21, 22</sup> EIS is, in principle, more accurate than CV in determining  $C_{dl}$ , because EIS can separate  $C_{dl}$  from possible pseudo-capacitances of chemisorption. In the presence of chemisorption, the FMG model expresses the total capacitance as,  $C_{total}(\omega) = C_{dl} + \frac{C_{ad}}{1 + \sqrt{j\omega\sigma_{ad}C_{ad} + j\omega C_{ad}R_{ad}}}$ , where  $C_{dl}$  is the pure double layer capacitance,  $R_{ad}$  adsorption resistance,  $C_{ad}$  adsorption capacitance,  $\sigma_{ad}$  coefficient of Warburg diffusional impedance,  $\omega$  angular frequency. Only when  $\omega \gg \omega_c = (C_{ad}R_{ad})^{-1}$  can one approximate  $C_{total}(\omega)$  as  $C_{dl}$ . At low frequencies, one will find

$C_{\text{total}}(\omega) \approx C_{\text{dl}} + C_{\text{ad}}$ . Earlier studies have shown that  $\omega_c$  is around 1 MHz for hydrogen adsorption at Pt(111) in 0.5 M perchloric acid,<sup>54</sup> and above 10 kHz for hydroxyl adsorption at Pt(111) in 0.1M perchloric acid.<sup>50</sup> A CV measurement with a scanning rate of  $50 \text{ mV s}^{-1}$  over a potential range of 0.05 V consumes 1 s, hence, has a characteristic frequency of 1 Hz, which is far lower than typical  $\omega_c$  of Pt(111) electrode processes. Ojha et al. reported the capacitance calculated from impedance at a single frequency of 18 Hz, which is also much below  $\omega_c$ .<sup>22</sup>

The fact that the CV-derived capacitance is much higher than the EIS-derived capacitance could be attributed to pseudo-capacitances of chemisorption. Based on this assumption, a theory for the large CV-derived capacitance of Pt(111) in the double layer region is developed in this paper. I am about to show that chemisorption at a few percentage of platinum sites can explain the observed large capacitance.

The remaining of this paper is organized as follows. Firstly, I present a short review of developments on the IHP model after the pioneering works of Grahame and Parsons.<sup>55, 56</sup> Most of these important works that adequately reflect the depth, core and beauty of electrochemical research are less known and only sparsely cited nowadays. This literature review also sets the baseline for the present model which is not entirely new, but extends previous models in some aspects. Secondly, a detailed derivation of model, including a water layer submodel and a chemisorption submodel, is presented. Thirdly, the model is demystified for two cases. In the first case without chemisorbed ions, emphasis is put on understanding how metal-water interactions change the pzc and the double layer capacitance. For the second case with chemisorbed ions, emphasis is put on the consequence of chemisorption-induced surface dipole moment. The model is then used to interpret recent experimental data of Ojha et al.<sup>21, 22</sup> in the double layer region. Fourthly, discussion on assumptions, implications and possible extensions of the model is presented before the conclusion section.

## Models of the IHP: Grahame-Parsons model and beyond.

Above analysis has turned the spotlight on the IHP in understanding the EDL at transition metals. *Figure 1* summarizes three groups of IHP models. The Grahame-Parsons model views the IHP as an ionic layer with specifically adsorbed ions rigidly lining up.<sup>55-57</sup> The potential drop from the metal surface to the IHP is composed of two parts. The first part is due to the metal surface charge, and the second part the net charge of specifically adsorbed ions at the IHP. There is no electron transfer during specific ionic adsorption, hence the specifically adsorbed ions retain the charge they have in the bulk solution. In the literature, e.g. ref.<sup>58</sup>, there is another Grahame-Parsons model which describes the thermodynamics of specific ion adsorption, and determines the coverage of adsorbed ion as a function of the electrode potential. The Grahame-Parsons model of ion adsorption was later improved by the Alekseev-Popov-Kolotyrkin model,<sup>59</sup> and the Vorotyntsev model.<sup>60</sup>

Another group of IHP models focus on solvent molecules at the IHP in the absence of specifically adsorbed ions, see *Figure 1* (b), see an earlier review by Guidelli.<sup>61</sup> The two-state model assumes that water molecules take either the hydrogen-up or hydrogen-down configuration, depending on the local electric field.<sup>34</sup> The three-state model further considers formation of water dimers and interconversion between water dimers and monomers.<sup>36</sup> Both models are founded purely on electrostatic considerations, thus the average dipole moment of the water layer is zero when the metal surface has a zero net charge. In addition to electrostatic interactions, chemical interactions between water molecules and the metal surface were speculated in the 1970s.<sup>62</sup> Damaskin and Frumkin considered both electrostatic and chemical metal-water interactions at the IHP.<sup>63</sup> Electrostatic interactions are treated using the approach of Bockris, Devanathan and Miller (BDM),<sup>64</sup> which does not consider properly the configurational entropy. The fraction of chemisorbed water molecules was expressed phenomenologically as an exponential function of the electrode charge. Recently, we have seen a surge of atomistic simulations of water molecules near metal surfaces, bringing about a much detailed picture of water dynamics at metal surfaces.<sup>53, 65-69</sup> These first-principles calculation results can be used to parameterize phenomenological models, as demonstrated in the work by Le et al.<sup>53</sup>

In most cases, the IHP is neither an ionic layer nor a solvent layer. Instead, it is a mixture of solvent molecules and chemisorbates. Chemisorbates, usually partially charged due to partial charge transfer, contribute an additional potential drop in the inner layer.<sup>70</sup> Therefore, a refined model of the IHP should be a binary IHP model that considers co-existing solvent molecules and partially charged chemisorbates. Carnie and Chan developed a so-called civilized model of EDLs which considers ions as hard spheres with embedded point charge, and solvent molecules as hard spheres with embedded dipole moment in the

1980s.<sup>71</sup> The Carnie-Chan model was used to calculate the dipole moment of specifically adsorbed ions at the IHP.<sup>72</sup> More recently, the binary IHP model was further extended to consider potential-varying coverage of partially charged chemisorbates.<sup>73, 74</sup> More than just a further complication of a model, it brings forth non-trivial implications of chemisorption-induced surface dipole moment ( $\mu_{\text{chem}}$ ). It was revealed that  $\mu_{\text{chem}}$  of adsorbed hydroxyl leads to a nonmonotonic surface charging behavior of Pt(111)-aqueous solution interfaces. Specifically, the free charge, not the total charge nor the metal charge,<sup>75</sup> exhibits a negative-positive-negative transition with increasing electrode potential. This implies the occurrence of negative  $C_{\text{dl}}$  and more than one potentials of zero free charge. Nonmonotonic surface charging behaviors of a polycrystalline Pt electrode were measured using the radioactive tracers method by Frumkin and co-workers,<sup>76, 77</sup> and later in several experiments of laser-induced potential transients.<sup>78-80</sup> The nonmonotonic surface charging behaviors were modelled earlier by assuming that the pzc grows linearly with the coverage of adsorbed oxygen, and later by a phenomenological treatment in which the potential drop in the IHP is interpolated between two limiting states.<sup>77</sup> The model developed in ref.<sup>73, 74</sup> and later modified in ref.<sup>81</sup> provides a consistent treatment of chemisorption and surface charging behaviors as a function of electrode potential. It was also shown in ref.<sup>73</sup> that orientational polarization of interfacial water molecules, described using the two state model, leads to a negative capacitive component to  $C_{\text{dl}}$ , an effect that was later elucidated in greater detail by Le et al.<sup>53</sup>

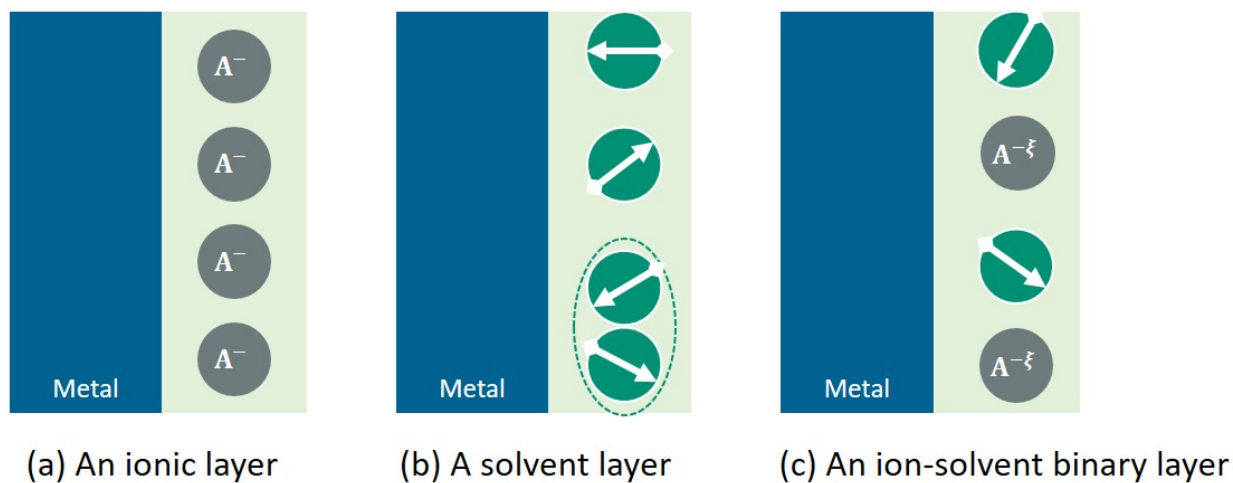


*Figure 1 Models of the inner Helmholtz plane (IHP). (a) The Grahame-Parsons model views the IHP as an ionic layer where specifically adsorbed ions are rigidly aligned.<sup>55-57</sup> (b) Many models are focused on the field-dependent behaviors of solvent molecules, most often water molecules, at the IHP.<sup>34, 36, 64</sup> (c) Recent models consider the coexistence of solvent molecules and partially charged chemisorbed ions ( $A^{-\xi}$ ) at the IHP.<sup>73, 74</sup>*

The IHP model that I am about to present in this paper improves over the previous one in ref.<sup>73, 74</sup> in three aspects. Firstly, the present model abandons the BDM-type two-state water model, and adopts a statistical treatment of water polarization with a continuum spectrum of orientational states, following the approach developed earlier in refs.<sup>82, 83</sup>. The configurational entropy of water molecules at the IHP is considered. In addition to electrostatic interactions, chemical interactions with the metal are considered, as inspired by *ab initio* molecular dynamics (AIMD) results,<sup>53, 67, 68</sup> but in a different manner compared to the Damaskin-Frumkin model. Secondly, chemisorption at the IHP is now energetically distributed in such a way that the equilibrium potential follows a distribution instead of taking a single value as usual. This allows to treat chemisorption at different types of active sites, chemisorption of different species, and lateral interactions between chemisorbates in a unifying manner. Thirdly, as suggested by recent detailed atomistic simulations, e.g., Ref.<sup>84</sup>, the IHP is further divided into an adsorbed ion plane (AIP) and an adsorbed solvent plane (ASP). This refinement is necessary because the AIP and ASP have very different properties, which I am about to show in model parameterization.

## Model development

### Physical picture of the double layer

A schematic illustration of an electrocatalytic double layer is presented in Figure 2 (a), and a continuum model is depicted in Figure 2 (b). The metal electrode is assumed to be planarly uniform. Surface roughness is not considered here. The first-layer water molecules are usually highly polarized due to the high interfacial electric field and chemical interactions with the metal, see a recent review by Groß and Sakong.<sup>69</sup> The ASP denotes the outer plane of adsorbed solvent molecules. Adsorbed ions, if any, are usually located closer to the metal surface than adsorbed solvent molecules, according to atomistic simulations, e.g., by Braunwarth, Jung, and Jacob.<sup>84</sup> The central plane of adsorbed ions is denoted AIP. Different characteristic planes are used for depicting the ASP and AIP due to difference between ionic charge and dipolar charge. Nonspecifically adsorbed ions with their solvation shell reside in the diffuse layer stretching from the OHP towards the solution bulk. The regions between the metal and the AIP, the AIP and the ASP, the ASP and the OHP are described as dielectric continua, parameterized with thicknesses  $\delta_i$  and permittivities  $\epsilon_i$ , with  $i = 1, 2, 3$ .

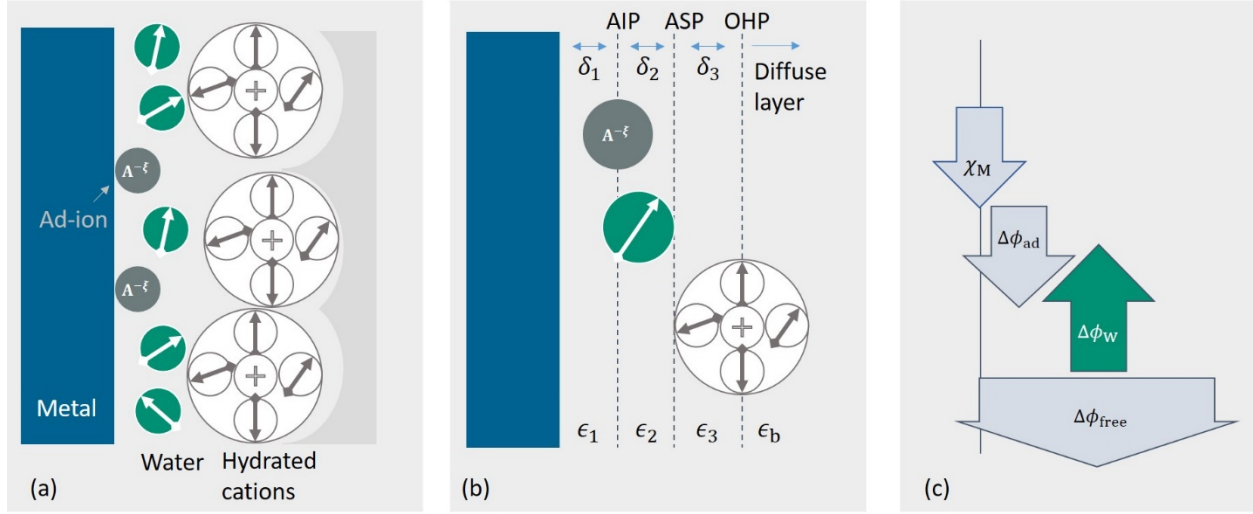


Figure 2 (a) Schematic illustration of the electrocatalytic double layer with partially-charged, chemisorbed ions, adsorbed solvent (water in this case) molecules, and nonspecifically adsorbed ions. (b) A continuum EDL model consists of an AIP denoting the central plane of chemisorbed ions, an ASP denoting the outer plane of adsorbed water molecules, and an OHP denoting the central plane of nonspecifically adsorbed ions. The regions between the metal and the AIP, the AIP and the ASP, the ASP and the OHP are described as dielectric continua, parameterized with thicknesses  $\delta_i$  and permittivities  $\epsilon_i$ , with  $i = 1, 2, 3$ . (c) The overall potential difference between the metal bulk and the solution bulk can be divided into four components:  $\chi_M$  denoting the potential drop at the metal surface due to electron distribution,  $\Delta\phi_{ad}$  the potential change due to partially-charged, chemisorbed ions,  $\Delta\phi_w$  the potential change due to orientational polarization of adsorbed water molecules, and  $\Delta\phi_{free}$  the potential change due to excess ionic charge stored in the diffuse layer, namely, free surface charge.

### Potential differences in different components

As EDL is a grand canonical system with electrode potential being one of independent variables, the overarching task of any EDL model is to calculate the electric potential distribution from the metal to the electrolyte solution. Figure 2 (c) depicts components of the overall potential difference between metal bulk ( $\phi_M$ ) and solution bulk ( $\phi_S$ ). At the metal surface exists a large potential drop due to the metal electron tail, denoted  $\chi_M$ , which is readily obtained from electronic structure calculations, e.g., in Ref.<sup>85</sup>. There are, at least, three other potential differences, including one due to partially-charged, chemisorbed



ions, one due to adsorbed solvent (water in this work) molecules, and one due to the free surface charge density,  $\sigma_{\text{free}}$ , defined as negative of the net ionic charge in the diffuse layer.<sup>81</sup>

The above decomposition scheme, following Ref.<sup>86</sup>, is expressed as,

$$\phi_M - \phi_S = \chi_M + \Delta\phi_{\text{free}} + \Delta\phi_{\text{ad}} + \Delta\phi_w \quad (1)$$

Within a continuum picture,  $\Delta\phi_{\text{free}}$  is written as

$$\Delta\phi_{\text{free}} = \text{sign}(\sigma_{\text{free}}) \frac{2RT}{F} \text{arsinh} \left( \sqrt{\frac{1}{2\gamma} \left( \exp \left( \frac{\gamma}{2} \left( \frac{F\lambda_D\sigma_{\text{free}}}{2RT\epsilon_b} \right)^2 \right) - 1 \right)} \right) + \sigma_{\text{free}} \sum_{i=1,2,3} \frac{\delta_i}{\epsilon_i} \quad (2)$$

where the first term denotes the potential change over the diffuse layer, which is derived from the Bikerman model considering finite ion size,<sup>28-74</sup>  $\lambda_D = \sqrt{\epsilon_b RT / 2c_b F^2}$  is the Debye length,  $\epsilon_b$  is the dielectric permittivity of the bulk solution,  $c_b$  is the bulk ion concentration,  $R$  is the gas constant,  $F$  is the Faraday constant,  $T$  is temperature,  $\gamma = 2c_b d_h^3$  with  $d_h$  being diameter of hydrated ions. Size asymmetry of cations and anions is not considered here, for the sake of an analytical expression of  $\Delta\phi_{\text{free}}$  as a function of  $\sigma_{\text{free}}$ , and effects of size asymmetry on the  $C_{\text{dl}}$  are known already.<sup>87-90</sup>

Other two components  $\Delta\phi_{\text{ad}}$  and  $\Delta\phi_w$  are determined from two submodels as introduced below.

### Distributed chemisorption model

The amount of charge carried by partially-charged, chemisorbed ions at the AIP is calculated as,  $-\sum_A N_{\text{ad}} \theta_A e_0 \xi_A$ , where  $N_{\text{ad}}$  is the number density of adsorption sites,  $\theta_A$  and  $\xi_A$  are the coverage and net electron of a chemisorbed ion of type A,  $e_0$  is the elementary charge.<sup>81</sup> The parameter  $\xi_A$  is related to the partial charge transfer coefficient,  $\lambda_A$ , via  $\xi_A = z_A + \lambda_A$ , with  $z_A$  being the initial charge of chemisorbed ions. A total charge transfer process corresponds to,  $\lambda_A = -z_A$ . Note in passing that the net charge  $\xi_A$  and the partial charge transfer coefficient  $\lambda_A$  are different from the electrosorption valency that can be measured experimentally.<sup>86</sup>

$\Delta\phi_{\text{ad}}$  is then calculated as the potential difference across an equivalent planar capacitor with a charge amount of  $\sum_A N_{\text{ad}} \theta_A e_0 \xi_A$  on each side,

$$\Delta\phi_{\text{ad}} = \frac{\delta_1}{\epsilon_1} \sum_A N_{\text{ad}} \theta_A e_0 \xi_A \quad (3)$$

A positive-valued  $\xi_A$  means negatively charged chemisorbed ions, which introduces a positive  $\Delta\phi_{\text{ad}}$ . A chemisorption submodel is required to determine  $\theta_A$  as a function of the electrode potential.

For chemisorption of hydrogen,  $H^+ + e + * \leftrightarrow H_{ad}$ , the Frumkin isotherm gives,<sup>91, 92</sup>

$$\ln\left(\frac{\theta_H}{\theta_{H,max} - \theta_H}\right) + \gamma_H \theta_H = -\beta(E_{RHE} - E_H^0) \quad (4)$$

where  $\theta_H$  is the coverage of  $H_{ad}$ ,  $\theta_{H,max}$  the maximum coverage,  $\gamma_H$  the lateral interaction coefficient,  $\beta = F/RT$ ,  $E_H^0$  the equilibrium potential on the standard hydrogen electrode (SHE) scale. Recently, Hormann et al. has illustrated how to obtain  $E_H^0$  and  $\gamma_H$  from density functional theory (DFT) calculations.<sup>93</sup> The existence of lateral interactions stands in the way of obtaining an analytical solution for  $\theta_H$ .

The Frumkin isotherm can be transformed to a series of Langmuir-type isotherms with a distributed  $E_H^0$ ,

$$\left\{ \ln\left(\frac{\theta_H}{\theta_{H,max} - \theta_H}\right) = -\beta(E_{RHE} - E), f_H(E) \right\} \quad (5)$$

where  $f_H(E)$  denotes the probability of an equilibrium potential at  $E$ .

The distribution in equilibrium potential can be ascribed to the existence of structural defects, lateral interactions that change the electrochemical potential for later adsorbates, a potential-dependent distribution in the electrochemical potential of reactants, among others. I will go back to this in the discussion section.

As any distribution can be expanded as a series of normal distributions,  $E_H^0$  is assumed to take the following general form,

$$f_H(E) = \sum_k p_k g_k(E; \mu_k, \sigma_k) \quad (6)$$

where  $g_k(E; \mu_k, \sigma_k)$  are normal distributions of weight  $p_k$ , expectations  $\mu_k$  and variances  $\sigma_k$

$$g_k(E; \mu_k, \sigma_k) = \frac{1}{\sigma_k \sqrt{2\pi}} \exp\left(-\frac{1}{2} \left(\frac{E - \mu_k}{\sigma_k}\right)^2\right) \quad (7)$$

and  $\sum_k p_k = 1$  for the weight values.

Now,  $\theta_H$  is expressed analytically as,

$$\theta_H = \int dE f_H(E) \theta_{H,max} \frac{\exp(-\beta(E_{RHE} - E))}{1 + \exp(-\beta(E_{RHE} - E))} \quad (8)$$

Similarly, the coverage of adsorbed OH is written as,

$$\theta_{\text{OH}} = \int dE f_{\text{OH}}(E) \theta_{\text{OH,max}} \frac{\exp(\beta(E_{\text{RHE}} - E))}{1 + \exp(\beta(E_{\text{RHE}} - E))} \quad (9)$$

where  $f_{\text{OH}}(E)$  is the distribution function of the equilibrium potential of OH adsorption, which has the same form of Eq.(6).

The pseudo-capacitance of chemisorption of  $\text{H}_{\text{ad}}$  and  $\text{OH}_{\text{ad}}$  is calculated as,

$$C_{\text{A}_{\text{ad}}} = \mp N_{\text{ad}} e_0 \frac{d\theta_{\text{A}}}{dE_{\text{RHE}}} \quad (10)$$

with  $\text{A} = \text{H} (-)$  or  $\text{OH} (+)$ .

Cautious readers may think a term  $(1 \pm \xi_{\text{A}})$  (+ for  $\text{H}_{\text{ad}}$  and  $-$  for  $\text{OH}_{\text{ad}}$ ) should be added in Eq.(10) to account for the partial charge transfer. This is unnecessary because no matter how the electron is partitioned between the metal and the adsorbate, one electron is taken out from or moved into the electrode, if  $\sigma_{\text{free}}$  is fixed.

The Frumkin isotherm can be regarded as a Langmuir isotherm with the equilibrium potential linearly varying with the adsorbate coverage, with the linear coefficient being the lateral interaction coefficient. In this sense, the distribution function expressed in Eq.(6) is just a generalization of the Frumkin isotherm. In fact, the linear coverage dependence of the equilibrium potential has no fundamental reason but is just a first approximation. Nonlinear effects have been observed in many cases such as the chemisorption of OH at Pt(111) in the study of Climent et al.<sup>92</sup> The exact form of  $f_{\text{A}}(E)$  corresponding to the Frumkin isotherm is unknown currently. However, I will extract  $f_{\text{H}}(E)$  and  $f_{\text{OH}}(E)$  from experimental CVs that are usually fitted using Frumkin isotherms.

### Water model with a continuous spectrum of orientational states

The last term in Eq.(1) is the potential difference due to average dipole moment of the first-layer water molecules,

$$\Delta\phi_{\text{w}} = -\frac{N_{\text{ad}}\theta_{\text{w}}}{\epsilon_2} \mu_{\text{w}} \langle \cos \alpha_{\text{w}} \rangle \quad (11)$$

where  $\theta_{\text{w}}$  is the coverage of water molecules,  $\mu_{\text{w}}$  is the dipole moment of a water molecule,  $\langle \cos \alpha_{\text{w}} \rangle$  is the statistical average of  $\cos \alpha_{\text{w}}$  with  $\alpha_{\text{w}}$  being the angle between water dipoles and the local

electric field, as depicted in *Figure 3*. Herein, a positive electric field points towards the bulk solution, and the direction of a dipole points from its negative end to its positive end.

In this model,  $\alpha_w$  could take any value between 0 and 180 degree, instead of two values in the Watts-Tobin model and the BDM model that were widely adopted in recent works.<sup>53, 73</sup> In this sense, the present treatment could be named an infinite-state water model.

Consider a canonical ensemble consisting of  $N_w$  water molecules at the IHP. At the mean-field level, the Hamiltonian of this canonical ensemble is written as,

$$\mathcal{H}_w = \sum_i (\mu_w E_{\text{loc}} + \delta\mu) \cos(\alpha_i) \quad (12)$$

where  $\alpha_i$  is the angle between the  $i^{\text{th}}$  water and the local electric field  $E_{\text{loc}} = -\frac{\sigma_{\text{free}}}{\epsilon_2}$ ,  $\delta\mu$  is the chemical interaction energy difference between the case of  $\alpha_w = 0^\circ$  and the case of  $\alpha_w = 180^\circ$ , see an illustration in *Figure 3* (a). The introduction of  $\delta\mu$  accounts for chemical interactions between water molecules and the metal surface. Damaskin and Frumkin also considered chemical metal-water interactions.<sup>63</sup> A key difference between this water model and the Damaskin-Frumkin model is that a statistical ensemble approach is adopted here.

The partition function of the water layer is written as,<sup>94</sup>

$$\mathcal{Z}_w = \frac{\int_0^{2\pi} \prod_i d\psi_i \int_0^\pi \prod_i d\alpha_i \sin \alpha_i \exp(-\mathcal{H}_w/k_B T)}{\left( \int_0^{2\pi} d\psi_i \int_0^\pi d\alpha_i \sin \alpha_i \right)^{N_w}} = \left[ \frac{\sinh((\mu_w E_{\text{loc}} + \delta\mu)/k_B T)}{(\mu_w E_{\text{loc}} + \delta\mu)/k_B T} \right]^{N_w} \quad (13)$$

where  $\psi_i$  is the longitude of the solid angle.

The Helmholtz free energy of the water layer is calculated as,

$$A_w = -k_B T \ln \mathcal{Z}_w = -k_B T N_w \ln \left[ \frac{\sinh((\mu_w E_{\text{loc}} + \delta\mu)/k_B T)}{(\mu_w E_{\text{loc}} + \delta\mu)/k_B T} \right] \quad (14)$$

The statistical average of  $\cos(\alpha_i)$  is calculated as,

$$\langle \cos \alpha_w \rangle = \frac{\int_0^{2\pi} \prod_i d\psi_i \int_0^\pi \prod_i d\alpha_i \sin \alpha_i \cos \alpha_i \exp\left(-\frac{\mathcal{H}_w}{k_B T}\right)}{\int_0^{2\pi} \prod_i d\psi_i \int_0^\pi \prod_i d\alpha_i \sin \alpha_i \exp\left(-\frac{\mathcal{H}_w}{k_B T}\right)} \quad (15)$$

$$= \frac{1}{N_w \mu_w} \frac{\partial A_w}{\partial E_{loc}} = -\coth\left(\frac{(\mu_w E_{loc} + \delta\mu)}{k_B T}\right) + \frac{1}{(\mu_w E_{loc} + \delta\mu)/k_B T}$$

### Surface charging formula

Combining Eqs.(1)(2) (3) and (11) leads to a formula from which one can solve for  $\sigma_{free}$  as a function of  $\phi_M$ ,

$$\begin{aligned} & \text{sign}(\sigma_{free}) \frac{2RT}{F} \text{arsinh}\left(\sqrt{\frac{1}{2\gamma} \left(\exp\left(\frac{\gamma}{2} \left(\frac{F\lambda_D \sigma_{free}}{2RT\epsilon_b}\right)^2\right) - 1\right)}\right) + \sigma_{free} \sum_{i=1,2,3} \frac{\delta_i}{\epsilon_i} \\ & + \frac{\delta_1}{\epsilon_1} \sum_A N_{ad} \theta_A e_0 \xi_A - \frac{N_{ad} \theta_w}{\epsilon_2} \mu_w \langle \cos \alpha_w \rangle + \chi_M = \phi_M - \phi_S \end{aligned} \quad (16)$$

At the pzc,  $\sigma_{free} = 0$ , Eq.(16) is thus simplified to,

$$(\phi_M - \phi_S)_0 = \chi_M + \frac{\delta_1}{\epsilon_1} \sum_A N_{ad} \theta_A e_0 \xi_A - \frac{N_{ad} \theta_w}{\epsilon_2} \mu_w \left( \coth(\delta\tilde{\mu}) - \frac{1}{\delta\tilde{\mu}} \right) \quad (17)$$

where the subscript 0 denotes the pzc condition.

If there is no chemisorbed ions at the pzc, Eq.(16) is further simplified to,

$$(\phi_M - \phi_S)_0 = \chi_M + \frac{N_{ad} \theta_w}{\epsilon_2} \mu_w \left( \coth(\delta\tilde{\mu}) - \frac{1}{\delta\tilde{\mu}} \right) \quad (18)$$

where the dimensionless  $\delta\tilde{\mu} = \frac{\delta\mu}{k_B T}$  is used.

The potential difference  $\phi_M - \phi_S$  at an electrode-electrolyte interface is not measurable without involving its counterpart at a reference electrode,<sup>95</sup> and must be differentiated from the electrode potential  $E$  in experiments.

### Conversion from $(\phi_M - \phi_S)$ to electrode potential

In potentiostatic experiments, one can control the potential of the working electrode (WE), namely, the metal in Figure 2 (a), with respect to a reference electrode (RE). The electrode potential is written as,  $E = \phi_M - \phi_{RE}$  with  $\phi_{RE}$  being the inner potential of the RE, up to an unimportant constant accounting for different work functions of WE and RE materials. The electrode potential could be rewritten as a difference between two potential differences,  $E = (\phi_M - \phi_S) - (\phi_{RE} - \phi_S)$ . Here, it is assumed that the RE is put in the same electrolyte with the working electrode, and  $\phi_{RE} - \phi_S$  is the potential difference

between the RE and the electrolyte solution. The reversible hydrogen electrode (RHE) belongs to this case. If the RHE is used as the RE,  $(\phi_M - \phi_S)$  becomes,

$$(\phi_M - \phi_S) = E_{\text{RHE}} + (\phi_{\text{RE}} - \phi_S)_{\text{RHE}} \quad (19)$$

where the subscript ‘RHE’ specifies the reference electrode. This equation can be related to the constant inner-potential DFT proposed recently by Melander.<sup>96</sup>

According to the Nernst equation, the potential difference of the RHE and that of the standard hydrogen electrode (SHE) are correlated as,

$$(\phi_{\text{RE}} - \phi_S)_{\text{RHE}} = (\phi_{\text{RE}} - \phi_S)_{\text{SHE}} - (\ln 10) \frac{RT}{F} \text{pH} \quad (20)$$

where  $(\phi_{\text{RE}} - \phi_S)_{\text{SHE}}$  is the value at the SHE.

Combined, Eqs.(19) and (20) lead to,

$$(\phi_M - \phi_S) = E_{\text{SHE}} + (\phi_{\text{RE}} - \phi_S)_{\text{SHE}} \quad (21)$$

given that  $E_{\text{SHE}} = E_{\text{RHE}} - (\ln 10) \frac{RT}{F} \text{pH}$ .

Substituting Eq.(21) into Eq.(16) gives

$$\begin{aligned} & \text{sign}(\sigma_{\text{free}}) \frac{2RT}{F} \text{arsinh} \left( \sqrt{\frac{1}{2\gamma} \left( \exp \left( \frac{\gamma}{2} \left( \frac{F\lambda_D \sigma_{\text{free}}}{RT\epsilon_b} \right)^2 \right) - 1 \right)} \right) + \sigma_{\text{free}} \sum_{i=1,2,3} \frac{\delta_i}{\epsilon_i} \\ & + \frac{\delta_1}{\epsilon_1} \sum_A N_{\text{ad}} \theta_A e_0 \xi_A - \frac{N_{\text{ad}} \theta_w}{\epsilon_2} \mu_w \langle \cos \alpha_w \rangle = E_{\text{SHE}} + (\phi_{\text{RE}} - \phi_S)_{\text{SHE}} - \chi_M \end{aligned} \quad (22)$$

where  $(\phi_{\text{RE}} - \phi_S)_{\text{SHE}} - \chi_M$  is, in general, a function of  $E_{\text{SHE}}$ .

### Double-layer and total capacitance

In the presence of chemisorption, it is important to distinguish two types of differential capacitance. The differential double-layer capacitance, corresponding to the free surface charge, is defined as,

$$C_{\text{dl}} = \frac{\partial \sigma_{\text{free}}}{\partial E} \quad (23)$$

The differential total capacitance, corresponding to the total surface charge  $\sigma_{\text{total}}$ , is the sum of  $C_{\text{dl}}$  and pseudo-capacitances given in Eq.(10),

$$C_{\text{total}} = C_{\text{dl}} + \sum_A C_{A_{\text{ad}}} \quad (24)$$

according to the relation between  $\sigma_{\text{total}}$ ,  $\sigma_{\text{free}}$ , and adsorption charge as discussed in Ref.<sup>75</sup>

### Model parameterization

The process of parameterizing a continuum EDL model is more or less a process connecting it to atomistic simulations using Kohn-Sham DFT, reactive force field molecular dynamics (MD), etc. The model contains four groups of parameters. The first group concerns about the multilayer structure and dielectric properties of the EDL. The second and third group describe adsorbed water molecules and chemisorbed ions, respectively. The last group defines material properties of the metal and the electrolyte solution.

The first group of parameters includes  $\epsilon_i$  and  $\delta_i$ . Recent years have witnessed detailed DFT and MD studies of Pt(111) electrodes with chemisorbed H and OH. Le et al. showed that the density of  $H_{\text{ad}}$  peaks at  $\sim 1 \text{ \AA}$  above the metal surface.<sup>68</sup> Braunwarth, Jung, and Jacob gave a bond length of  $1.05 \text{ \AA}$  for adsorbed O on Pt(111).<sup>84</sup> Therefore, I use  $\delta_1 = 1 \text{ \AA}$  for the AIP. In the presence of an electron tail in the space between the metal and the AIP,  $\epsilon_1$  should be higher than the vacuum permittivity  $\epsilon_0$ , otherwise,  $C_{\text{dl}}$  is bounded by  $C_{\text{AIP}} = 8.85 \mu\text{F cm}^{-2}$ . Herein, I assume  $\epsilon_1 = 10\epsilon_0$  to account for the effects of valence electrons from Pt(111). These studies also indicated that the adsorbed, first-layer water molecules are around  $2.1 \text{ \AA}$  above the metal surface. Therefore,  $\delta_2$ , thickness of the gap between the AIP and ASP, is approximated as  $\delta_2 = 1.1 \text{ \AA}$ . Since orientational (inertial, slow, low-frequency) polarization of water dipoles is explicitly considered in  $\Delta\phi_w$ ,  $\epsilon_2$  is the electronic (noninertial, fast, high-frequency) permittivity, which is known to be  $\epsilon_2 = 3.25 \epsilon_0$  at room temperature.<sup>97</sup> Le et al. <sup>68</sup> used  $\epsilon_2 = 4\epsilon_0$ . An earlier estimate by Bockris, Devanathan and Muller reads  $\epsilon_2 = 6\epsilon_0$ .<sup>98</sup> For the region between the ASP and OHP, I used  $\delta_3 = 3.5 \text{ \AA}$ , a typical radius of hydrated ions, and  $\epsilon_3 = 78.5 \epsilon_0$ , the permittivity of bulk solution.

As for adsorbed water molecules, Le et al. determined a coverage of  $\sim 0.5$ .<sup>53</sup> Hence, I use  $\theta_w = 0.5$ . Schnur and Groß calculated the adsorption energy of the H-down and H-up water at several solids using an ice-like water bilayer model.<sup>99</sup> The H-down and H-up configurations correspond to  $\alpha_w = 180^\circ$  and  $\alpha_w = 0^\circ$ , respectively. Their data show that  $\delta\tilde{\mu} \approx 0$  at Ru(0001), and  $\delta\tilde{\mu} \approx 1$  at Au(111), Ag(111), and Pt(111). In more recent AIMD simulations, a more detailed picture of interfacial water molecules has emerged.<sup>53, 67, 100</sup> At the Pt(111)-water interface, a fraction of water molecules are bound strongly through their oxygen atom with the metal so that the hydrogen atoms of the water

molecule are above the oxygen atom. This is called the O-down configuration, corresponding to  $\alpha_w = 0^\circ$  in this model. A bit further away from the metal surface are resided another type of water molecules which can be further divided into the H-down ( $\alpha_w = 180^\circ$ ) and H-up ( $\alpha_w = 0^\circ$ ) configurations. The AIMD results suggest  $\delta\tilde{\mu} < 0$  in the present model. The intrinsic dipole moment of a water molecule is 1.85 D. However, in order to reproduce the permittivity of bulk water using the dipolar Poisson-Boltzmann theory, Abrashkin et al. used an effective value of 4.86 D.<sup>101</sup> Herein, I determine  $\mu_w$  from the interfacial potential change due to water orientation, which was determined to be -0.2 V for a clean, uncharged Pt(111) surface by Le et al.<sup>66</sup> From Eq.(22), the present model determines the orientation-induced potential change as  $\frac{N_{ad}}{\epsilon_2} \theta_w \mu_w \left( \coth(\delta\tilde{\mu}) - \frac{1}{\delta\tilde{\mu}} \right)$ . Assuming  $\delta\tilde{\mu} = -1$ , I thus determine  $\mu_w = \frac{-0.2\epsilon_2}{N_{ad}\theta_w(\coth(-1)+1)} = 0.73$  D. If  $\delta\tilde{\mu} = -2$ ,  $\mu_w = 0.43$  D. The lower bound of  $\mu_w$  is 0.23 D. A lower effective value of  $\mu_w$  accounts for unevenness of the first-layer water molecules, as well as offset effects by second-layer water molecules.

Malek and Eikerling calculated the work function change due to chemisorbed oxygen at Pt(111), from which they estimated the partial charge residing on each adsorbed oxygen.<sup>102</sup> Using a vacuum permittivity, they determined that each adsorbed oxygen on Pt(111) carries a partial charge of  $\sim 0.012e$ . Since  $\epsilon_1 = 10\epsilon_0$  is used here, I should use  $\xi_{OH} = 0.12$  to reproduce the same magnitude of work function change induced by chemisorbed ions. Chemisorbed H is assumed to be electroneutral, namely,  $\xi_H = 0$ . The present model does not need a single-valued equilibrium potential and lateral interaction coefficient. Instead, this model only needs  $f_H(E)$  and  $f_{OH}(E)$ , which are determined from experimental CVs.

With Pt(111) as the metal, I have  $N_{ad} = 0.15 \text{ \AA}^{-2}$  based on a lattice constant of  $3.92 \text{ \AA}$ , and the potential of zero charge is  $E_{pzc} = 0.29 \text{ V}_{SHE}$ .<sup>103</sup> Given that water dipole orientation lowers the pzc by 0.2 eV,  $E_{pzc}^0$  without considering this water dipole effect should be  $0.49 \text{ V}_{SHE}$ . In accordance with experiments by Ojha et al.,<sup>21, 22</sup> I consider an electrolyte solution of  $0.1 \text{ mM HClO}_4 + x \text{ mM LiClO}_4$ . The diameter of hydrated cations and anions is taken uniformly as  $d_h = 0.7 \text{ \AA}$ .

## The case without chemisorbed ions

The central formula expressed in Eq.(22) contains the interplay between the diffuse layer, water molecules at the ASP, and partially charged chemisorbed ions at the AIP. To simplify the matter, I consider in this section a simple case without chemisorbed ions, namely,  $\theta_A = 0$  in Eq.(22). The focus is



put on how chemical interactions between adsorbed water molecules and the metal influence the pzc, and furthermore how field-dependent reorientation of water molecules changes the  $C_{dl}$  profile.

### Influence of metal-water interactions on the pzc

In absence of chemisorbed ions, the pzc is obtained from Eq.(22) as,

$$E_{pzc,SHE} = \chi_M - (\phi_{RE} - \phi_S)_{SHE} + \frac{N_{ad}}{\epsilon_2} \theta_w \mu_w \left( \coth(\delta \tilde{\mu}) - \frac{1}{\delta \tilde{\mu}} \right) \quad (25)$$

where the first term is the potential drop at the metal surface determined by the electron density profile at the interface, the second term is a constant of the SHE, and the third term represents the influence of water molecules at the ASP.

$E_{pzc,SHE}^0$  is defined as the value for the case of  $\delta \tilde{\mu} = 0$ , namely, the case in which metal-water interactions are the same for water molecules possessing  $\alpha_w = 0^\circ$  and  $\alpha_w = 180^\circ$ . This artificial case is hardly met. In the general case of  $\delta \tilde{\mu} \neq 0$ , I obtain,

$$E_{pzc,SHE} = E_{pzc,SHE}^0 + \frac{N_{ad}}{\epsilon_2} \theta_w \mu_w \left( \coth(\delta \tilde{\mu}) - \frac{1}{\delta \tilde{\mu}} \right) \quad (26)$$

where the second term on the right hand side represents the pzc shift due to orientational polarization of adsorbed water molecules. It is important to emphasize that the pzc shift due to electronic polarization of adsorbed water molecules is included in  $E_{pzc,SHE}^0$ .

When  $|\delta \tilde{\mu}| \leq 1$ ,  $E_{pzc,SHE}$  is asymptotic to,

$$E_{pzc,SHE} = E_{pzc,SHE}^0 + \frac{N_{ad} \theta_w \mu_w}{3 \epsilon_2} \delta \tilde{\mu} \quad (27)$$

Eq.(27) implies that  $E_{pzc,SHE}$  is greater (smaller) than  $E_{pzc,SHE}^0$  when  $\delta \tilde{\mu} > 0$  ( $< 0$ ), as shown in Figure 3 (b). For the case of  $\delta \tilde{\mu} < 0$ , the first-layer water molecules prefer the  $\alpha_w = 0^\circ$  (H-up or O-down) configuration. For this case, the resulting potential rise due to the water dipole moment compensates partly the potential drop at the metal surface, leading to a smaller  $E_{pzc,SHE}$ . In the opposite case, the first-layer water molecules prefer the  $\alpha_w = 180^\circ$  (H-down) configuration, resulting in an additional potential drop and thereby a higher  $E_{pzc,SHE}$ .

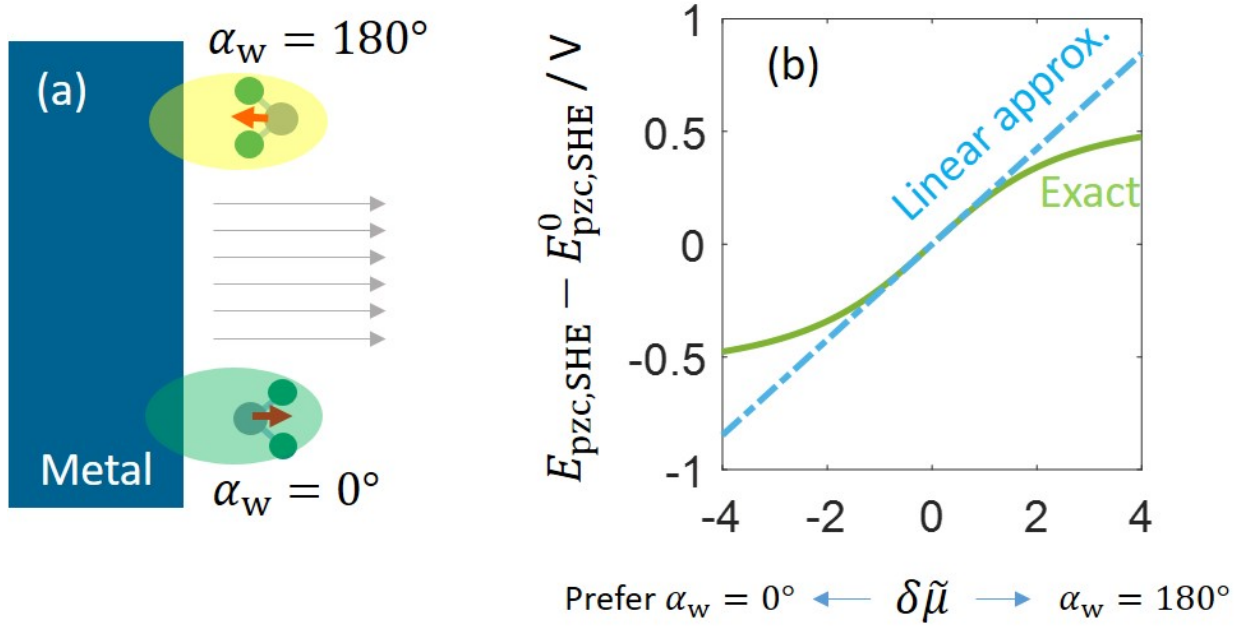


Figure 3 (a)  $\alpha_w$  is the angle between water dipoles and the local electric field. A positive electric field points towards the bulk solution, and the direction of a dipole points from its negative end to its positive end. Chemical metal-water interactions result in an energy difference between water of  $\alpha_w = 0^\circ$  and that of  $\alpha_w = 180^\circ$ , denoted  $\delta\mu$ . (b) Shift in the potential of zero charge as a function of  $\delta\tilde{\mu}$  (the solid line: exact results, the dotted line: linear approximation). The calculation uses the following set of model parameters:  $N_{ad} = 0.15 \text{ \AA}^{-2}$ ,  $\theta_w = 0.5$ ,  $\epsilon_2 = 3.25\epsilon_0$ ,  $\mu_w = 0.73 \text{ D}$ , as discussed in the model parameterization section. Matlab script of this figure is provided in the supporting material of this paper.

### Influence of water orientational polarization on $C_{dl}$

In this section, I analyze how water orientational polarization affects the differential double-layer capacitance  $C_{dl}$ . In addition to the full model, two simplified models are introduced to differentiate multiple coupled effects. The simplified model without ion size effects is described by a variant of Eq.(22) in the limit of  $\gamma = 0$ ,

$$\frac{2RT}{F} \operatorname{arsinh}\left(\frac{F\lambda_D\sigma_{free}}{2RT\epsilon_b}\right) + \sigma_{free} \sum_{i=1,2,3} \frac{\delta_i}{\epsilon_i} - \frac{N_{ad}}{\epsilon_2} \theta_w \mu_w \langle \cos \alpha_w \rangle = E_{SHE} - E_{pzc,SHE}^0 \quad (28)$$

In Eq.(28) I have neglected the chemisorption-induced dipole moment for this case without chemisorbed ions. The simplified model without water effects is expressed as a variant of Eq.(22) in the limit of  $\theta_w = 0$ ,

$$\begin{aligned} \text{sign}(\sigma_{\text{free}}) \frac{2RT}{F} \text{arsinh} \left( \sqrt{\frac{1}{2\gamma} \left( \exp \left( \frac{\gamma}{2} \left( \frac{F\lambda_D \sigma_{\text{free}}}{RT\epsilon_b} \right)^2 \right) - 1 \right)} \right) + \sigma_{\text{free}} \sum_{i=1,2,3} \frac{\delta_i}{\epsilon_i} \\ = E_{\text{SHE}} - E_{\text{pzc,SHE}}^0 \end{aligned} \quad (29)$$

In Figure 4, I compare the three models for the case of  $\delta\tilde{\mu} = 0$  with the base set of model parameters. The model without water effects has a camel-shaped  $C_{\text{dl}}$  curve with two very broad peaks corresponding to overcrowding of counterions. The  $C_{\text{dl}}$  curve is symmetric around the pzc as I have neglected size asymmetry. Otherwise, the peak corresponding to smaller counterions will be higher, see, e.g., Ref.<sup>27</sup>.

Upon an increment in the magnitude of  $\sigma_{\text{free}}$ , adsorbed water molecules at the ASP could reduce the potential drop across the EDL via rearranging their orientations. Consequently,  $C_{\text{dl}}$  is increased due to water polarization effects, as seen in the comparison between the full model and the model without water effects. Equivalently, water molecules at the ASP contribute a negative capacitance in series with the diffuse layer capacitance, as pointed out earlier by Huang et al.<sup>73</sup> and Le et al.<sup>53</sup>

The two peaks of the  $C_{\text{dl}}$  curve become sharper and move closer to the pzc, compared to their counterparts of the model without water effects. The two peaks signify saturation of water polarization effect, rather than overcrowding of counterions in previous modified Poisson-Boltzmann theories.<sup>28, 29</sup> Mathematically, it corresponds to  $\langle \cos \alpha_w \rangle = 1$  or  $-1$  depending on the sign of  $\sigma_{\text{free}}$ . These two peaks are significantly elevated when  $\mu_w$  increases from the base value of 0.73D to 0.9 D, as shown in Figure 4(b).

Since the electrolyte solution is ultra-dilute,  $c_0 = 0.1$  mM, the ion size effect is unimportant near the pzc as the  $C_{\text{dl}}$  curves of the full model and the model without ion size effects overlap in the region of  $|E_{\text{SHE}} - E_{\text{pzc,SHE}}^0| < 0.2$  V. As  $\sigma_{\text{free}}$  grows in magnitude and the EDL becomes more crowded with counterions, the ion size effect cannot be neglected any longer. Without considering the ion size effect, the two peaks are higher.

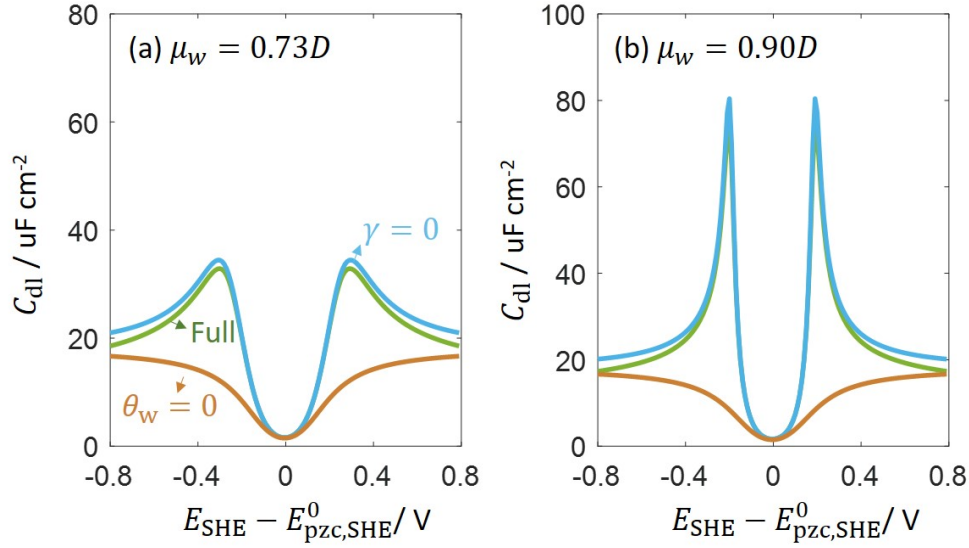


Figure 4 Differential double layer capacitance as a function of the electrode potential for the case of  $\delta\tilde{\mu} = 0$  for two effective values of water dipole moment: (a)  $\mu_w = 0.73 D$ , (b)  $\mu_w = 0.90 D$ .  $E_{pzc,SHE}^0$  represents the potential of zero charge without water dipole effects, which is used as the electrode potential reference here. Three models, including the full model, a simplified model without ion size effects, and a simplified model without water effects. The electrolyte solution is 0.1 mM  $HClO_4$ .  $\delta\tilde{\mu} = 0$ , and other model parameters have their base values. Matlab script of this figure is provided in the supporting material of this paper.

Figure 5 (a) examines the influence of  $\delta\tilde{\mu}$  on the  $C_{dl}$  curve. As already discussed, the pzc, corresponding to the valley of the  $C_{dl}$  curve, shifts to more negative electrode potentials as  $\delta\tilde{\mu}$  goes negative. The  $C_{dl}$  curve becomes highly asymmetric with the left peak being much higher than the right one for  $\delta\tilde{\mu} = -1$ . A negative  $\delta\tilde{\mu}$  means that in the absence of electrostatic interactions, water molecules prefer the configuration of  $\alpha_w = 0^\circ$  (the O-down or H-up configurations). Therefore, these water molecules have a higher capacity to screen negative  $\sigma_{free}$ , that intends to rotate water molecules towards  $\alpha_w = 180^\circ$ , than positive  $\sigma_{free}$ . Consequently, a higher  $C_{dl}$  peak is observed in the negatively charged region. Interestingly, a more symmetric  $C_{dl}$  curve is reobtained for  $\delta\tilde{\mu} = -6$ . For the case of such a very negative  $\delta\tilde{\mu}$ , the orientation of water molecules is dominated by the strong chemical interactions and is no longer tunable by the local electric field. Therefore, the  $C_{dl}$  curve resembles that of the model without water effects in Figure 4, except a horizontal shift due to  $\delta\tilde{\mu}$ .

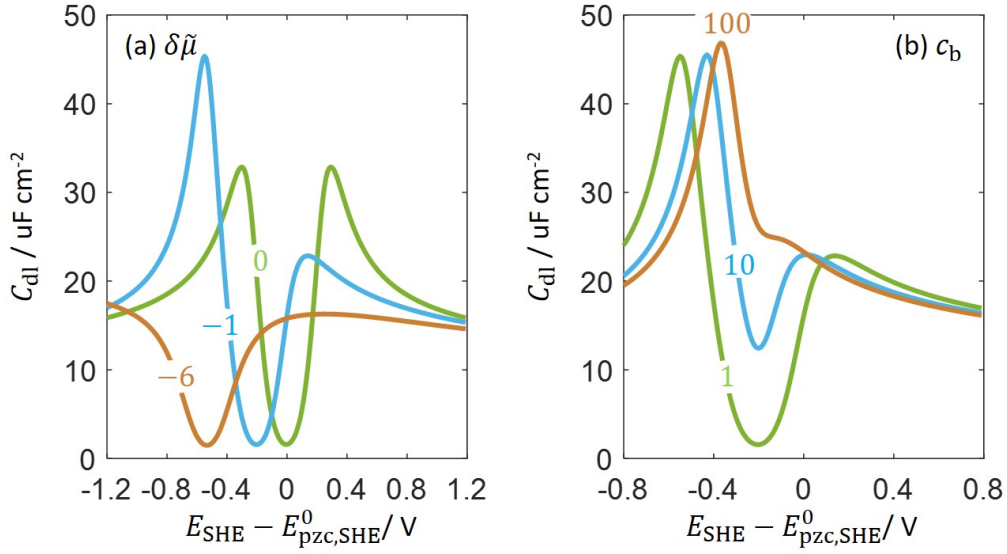


Figure 5 Differential double layer capacitance as a function of electrode potential for (a) different values of  $\delta\tilde{\mu}$  normalized to thermal energy  $k_B T$  when the electrolyte concentration is 0.1 mM, and (b) different electrolyte concentrations when  $\delta\tilde{\mu} = -1$ .  $E_{\text{pzc,SHE}}^0$  represents the potential of zero charge without water dipole effects, which is used as the electrode potential reference here. Other model parameters have their base values. Matlab script of this figure is provided in the supporting material of this paper.

Figure 5 (b) examines the concentration dependence of the  $C_{\text{dl}}$  curve while  $\delta\tilde{\mu} = -1$  is fixed.  $C_{\text{dl}}$  near the pzc is higher because the Debye length becomes smaller as the electrolyte concentration increases. In addition, the two peaks come closer in more concentrated electrolyte solution. These peaks are ascribed to saturation of water polarization. Let us denote as  $\sigma_{\text{free}}^c$  the critical magnitude of  $\sigma_{\text{free}}$  leading to saturated water polarization. At higher concentrations,  $C_{\text{dl}}$  is higher and  $\sigma_{\text{free}}^c$  can be achieved at a smaller potential difference away from the pzc.

## The case with chemisorbed ions

### Effect of chemisorption-induced dipole moment

Now chemisorption is brought into the play and its influence on the  $C_{\text{dl}}$  curve is examined. Let us consider the Pt(111)-0.1 M  $\text{HClO}_4$  interface. The CV of this interface is usually divided into a hydrogen adsorption region up to  $\sim 0.4 \text{ V}_{\text{RHE}}$ , a hydroxyl adsorption region above  $\sim 0.55 \text{ V}_{\text{RHE}}$ , and a double layer region inbetween. Climent et al. has conducted a comprehensive analysis of CVs of this interface at

different temperatures using Frumkin isotherms.<sup>92</sup> Herein, a revisit from a different view assuming distributed equilibrium potentials of  $H_{ad}$  and  $OH_{ad}$  is presented, with the focus put on the effect of chemisorption-induced dipole moment on  $C_{dl}$ .

Figure 6(a) shows a model fitting of the CV within the potential range of  $[0.15, 0.75]V_{RHE}$ , and a model-based decomposition of the total capacitance  $C_{tot}$  into  $C_{dl}$  and adsorption capacitances ( $C_{H_{ad}}$  and  $C_{OH_{ad}}$ ). The extracted distribution functions  $f_H$  and  $f_{OH}$ , defined in Eq.(6), are shown in Figure 6(b).  $f_H$  is composed of four Gaussian functions with preset mean values of 0, 0.1, 0.2, and 0.3  $V_{RHE}$ , and  $f_{OH}$  is composed of two Gaussian functions with preset mean values of 0.7 and 0.8  $V_{RHE}$ . Twelve free parameters are therefore the variances  $\sigma_k$  and weights  $p_k$  of these six distributions. Other EDL parameters have their base values. The basic idea of this approach resembles that of the distribution of relaxation times (DRT) proposed by von Schweidler in 1907, see a recent review on DRT.<sup>104</sup> The present approach could be termed distribution of chemisorption energies (DCE). A better fitting of  $C_{tot}$  can be obtained if a greater number of Gaussian functions are included, which is not the purpose of this work. The mere purpose of this fitting is to confirm that a Frumkin isotherm with repulsive lateral interactions can be mapped into a series of Langmuir isotherms with a DCE.

Figure 6(a) indicates that  $C_{dl}$  is a few percentage of  $C_{tot}$ . Figure 6(c) shows  $C_{dl}$  for the cases with and without  $\Delta\phi_{ad}$  caused by chemisorption. Three values of the net electron number of  $OH_{ad}$ ,  $\xi_{OH}$ , are compared, including the base value of 0.12, a zero value corresponding to the case of a complete charge transfer during chemisorption and hence a zero  $\Delta\phi_{ad}$ , and also a higher value of 0.20 to increase the magnitude of  $\Delta\phi_{ad}$ . When  $\Delta\phi_{ad} = 0$ , the  $C_{dl}$  curve contains a higher peak at  $\sim 0.2 V_{RHE}$ , and a much depressed peak at potentials more positive than  $E_{pzc} = 0.29 V_{SHE}$  ( $0.346 V_{RHE}$  for this case), similar to the results shown in *Figure 5* (b). In comparison,  $C_{dl}$  drops above 0.5  $V_{RHE}$  due to a positive  $\Delta\phi_{ad}$  when  $\xi_{OH} = 0.12$ . Particularly, negative  $C_{dl}$  is found when  $\xi_{OH} = 0.20$ .

Negative  $C_{dl}$  means that  $\sigma_{free}$  decreases with increasing electrode potential, resulting in a nonmonotonic surface charging behavior. Chemisorption-induced nonmonotonic surface charging behaviors were revealed in a previous work,<sup>73</sup> and elucidated in a, hopefully, more accessible manner recently by this writer.<sup>81</sup> The basic idea, as expressed in Eq.(1), is that negatively charged chemisorbed OH introduce a potential drop  $\Delta\phi_{ad}$ , which is tantamount to increasing the pzc. As a result,  $\sigma_{free}$  increases at a lower rate with the electrode potential, namely, a smaller  $C_{dl}$ , or decreases with the electrode potential, namely, a negative  $C_{dl}$ , depending on the magnitude of  $\mu_{OH}$ .

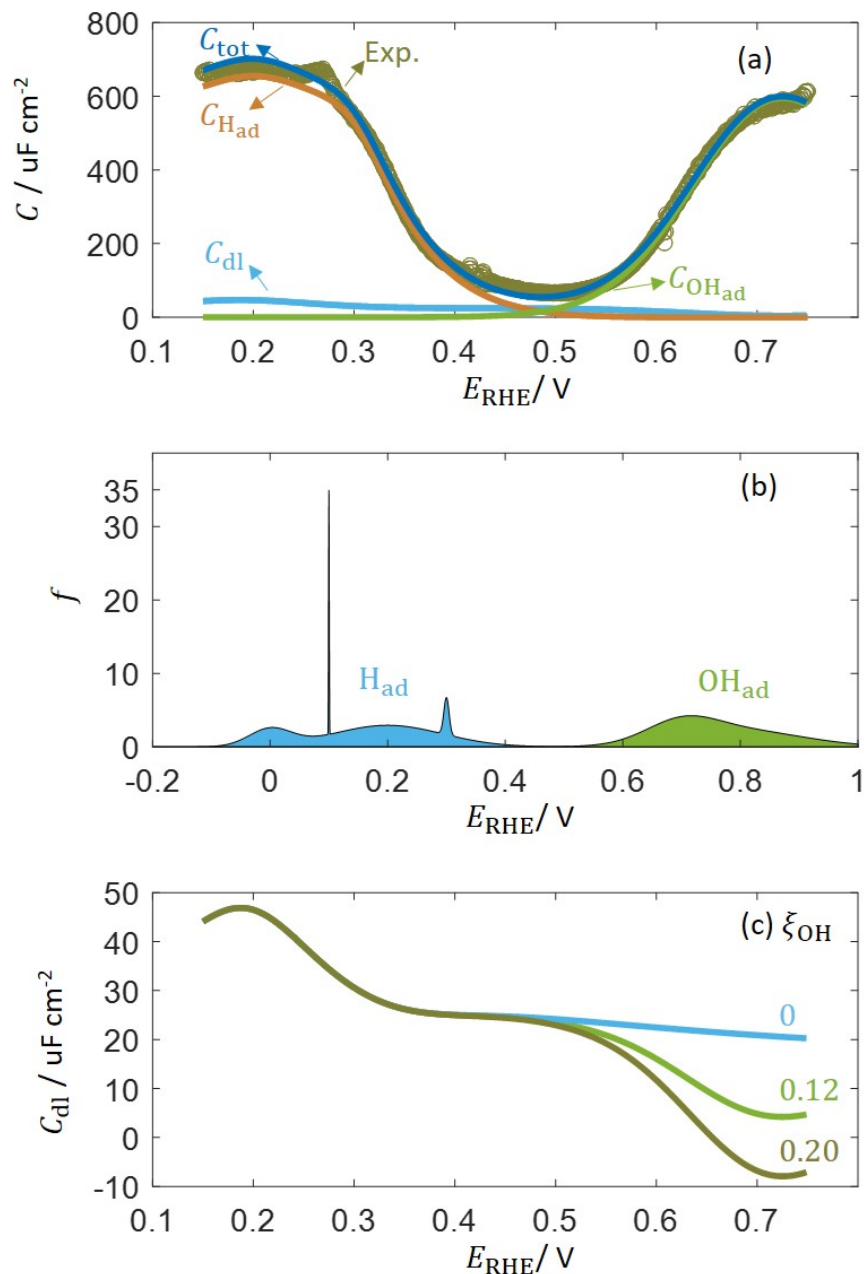


Figure 6 (a) Differential double-layer capacitance ( $C_{\text{dl}}$ ), adsorption capacitance of  $\text{H}_{\text{ad}}$  and  $\text{OH}_{\text{ad}}$  ( $C_{\text{H}_{\text{ad}}}$ ,  $C_{\text{OH}_{\text{ad}}}$ ), and their sum ( $C_{\text{tot}}$ ) for the double layer of Pt(111)-0.1 M  $\text{HClO}_4$  interface. Experimental data, shown in cricles ( $\circ$ ), are taken from Ref. <sup>22</sup>. (b) Model-based distributions of equilibrium potential of H and OH adsorption. (c) Comparison of differential double-layer capacitance for three values of the net electron number of  $\text{OH}_{\text{ad}}$ . The case of  $\xi_{\text{OH}} = 0$  corresponds to the case without chemisorption-induced dipole moment,  $\mu_{\text{OH}}$ . Matlab script of this figure is provided in the supporting material of this paper.

## The double layer region

Let us proceed to analyze recent experimental data by Ojha, Doblhoff-Dier and Koper, focusing on the double layer region between 0.40 and 0.65  $V_{\text{RHE}}$ .<sup>22</sup> In order to distance the pzc as much as possible from the hydrogen and hydroxyl adsorption/desorption regions, they delicately used 0.1 mM  $\text{HClO}_4$  as the base electrolyte solution with a pH of 4, where the pzc is 0.53  $V_{\text{RHE}}$ . They repeated the measurements on the Pt(111)- 0.1 mM  $\text{HClO}_4$  interface for three times, allowing us to examine how experimental uncertainties affect model results in *Figure 7*. Afterwards, experimental data in the presence of different concentrations of  $\text{LiClO}_4$  are analyzed in *Figure 8*.

Figure 7 (a)-(c) shows the model-experiment comparison for three pieces of capacitance data in 0.1 mM  $\text{HClO}_4$ . The EDL parameters are fixed at their base values, and the free fitting parameters are the weight  $p_k$ , expectations  $\mu_k$  and variances  $\sigma_k$  of distribution functions of  $\text{H}_{\text{ad}}$  and  $\text{OH}_{\text{ad}}$ . One Gaussian distribution for  $\text{H}_{\text{ad}}$  and two for  $\text{OH}_{\text{ad}}$  are sufficient in this narrow potential region. The fitted distributions are displayed in Figure 7 (d)-(f). The coverages of  $\text{H}_{\text{ad}}$  and  $\text{OH}_{\text{ad}}$  are shown in Figure 7 (g)-(i).

In Figure 7 (a)-(c), solid lines represent model results, and circles represent experimental data. The total capacitance ( $C_{\text{total}}$ ) is further decomposed, with the aid of the model, into the capacitance due to H adsorption,  $C_{\text{H}_{\text{ad}}}$ , that due to OH adsorption,  $C_{\text{OH}_{\text{ad}}}$ , and the pure double-layer capacitance,  $C_{\text{dl}}$ . The measured capacitance  $C_{\text{total}}$  is contributed majorly by pseudo-capacitances  $C_{\text{H}_{\text{ad}}}$  and  $C_{\text{OH}_{\text{ad}}}$ . Three measurements show a moderate difference inbetween: the terrace in the potential range of 0.55 – 0.6  $V_{\text{RHE}}$ , attributed to water adsorption in Ref.<sup>22</sup>, almost disappears in the third measurement.

The present model attributes different profiles of  $C_{\text{total}}$  to variations in the distributed equilibrium potential of  $\text{OH}_{\text{ad}}$ ,  $f_{\text{OH}}$ , as shown in Figure 7 (d)-(f). The OH adsorption has a bimodal normal distribution and the one at lower potentials with  $p_1 < 6\%$  is responsible for the terrace of  $C_{\text{total}}$  in the potential range of 0.55 – 0.6  $V_{\text{RHE}}$ . The terrace appears when the two normal distributions are well resolved, as in Figure 7 (d) and (e), and disappears when they come closer and become connected, as in Figure 7 (f). The variations in  $f_{\text{OH}}$  implies that the assumed distribution of equilibrium potential is likely affected by stochastic factors.

The coverages of adsorbed  $\text{H}_{\text{ad}}$  and  $\text{OH}_{\text{ad}}$ , denoted  $\theta_{\text{H}}$  and  $\theta_{\text{OH}}$ , are less than 5% in the double-layer region. However, such a small amount of adsorption results in adsorption capacitance several fold higher than  $C_{\text{dl}}$ , which demonstrates the importance of and also difficulty in separating  $C_{\text{dl}}$  from adsorption capacitances for electrocatalytic double layers.



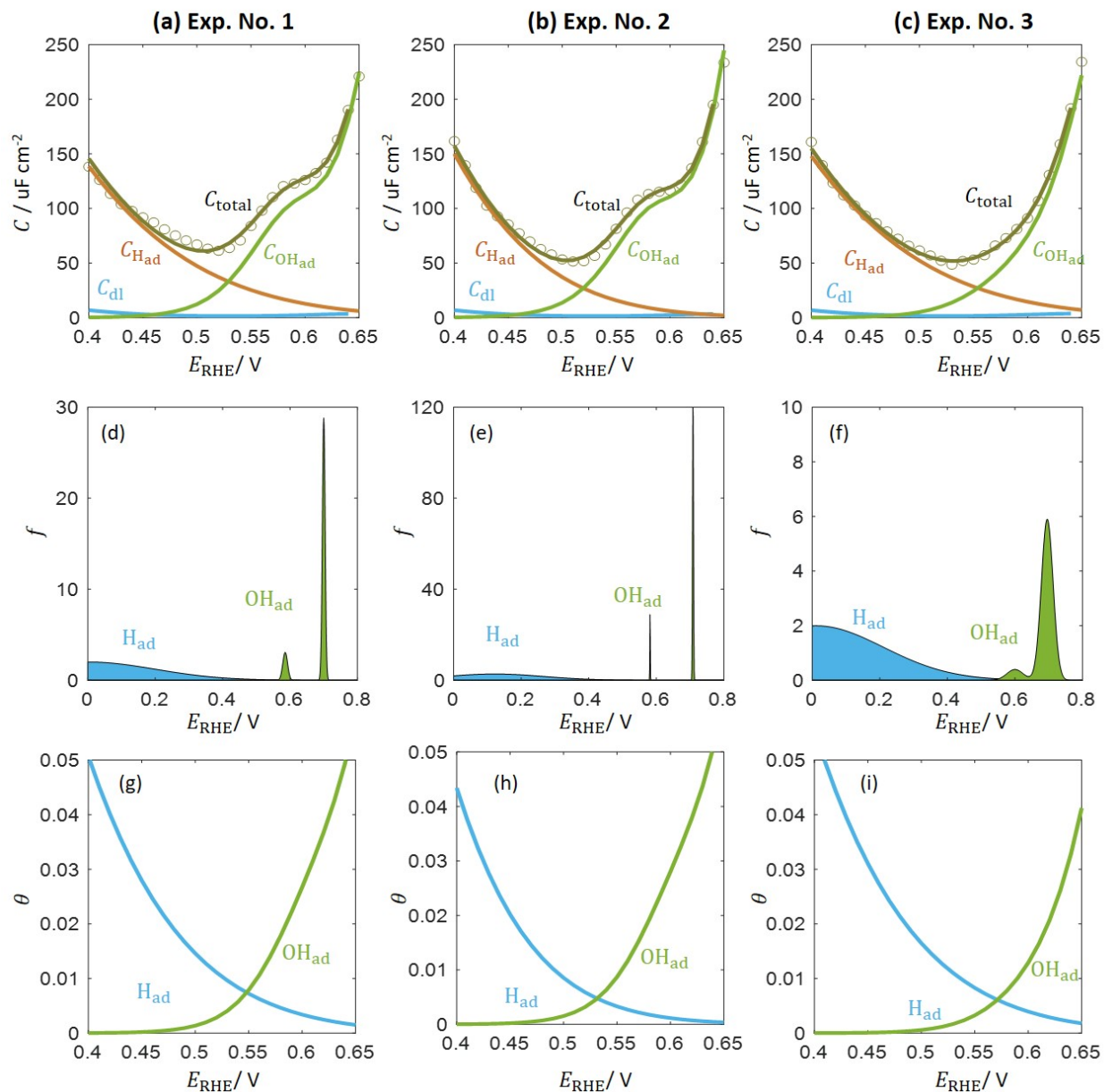


Figure 7 (a)-(c) Model-experiment comparison for the electric double layer at Pt(111)-aqueous interfaces. The experiment on a Pt(111) electrode in 0.1 mM HClO<sub>4</sub>, was repeated three times.<sup>22</sup> Model results are marked as solid lines, and experimental data circles. The total capacitance ( $C_{\text{total}}$ ) is decomposed into the capacitance due to H adsorption,  $C_{\text{H}_{\text{ad}}}$ , that due to OH adsorption,  $C_{\text{OH}_{\text{ad}}}$ , and the pure double-layer capacitance,  $C_{\text{dl}}$ . (d)-(f) Model-based distributions of the equilibrium potential of H and OH adsorption. (g)-(i) Coverages of adsorbed H and OH. Matlab script of this figure is provided in the supporting material of this paper.

Experimental data in the presence of different concentrations of  $\text{LiClO}_4$  are analyzed in Figure 8. The experiments were conducted on a Pt(111) in  $0.1 \text{ mM HClO}_4 + x \text{ mM LiClO}_4$  ( $x=0.1, 0.3, 0.6, 1.0$ ).<sup>22</sup> Experimental capacitance curves are shifted vertically in Figure 8(a) for visual clarity. The model results in solid lines neatly agree with experimental data in circles in the examined potential region. The fitted coverages of  $\text{H}_{\text{ad}}$  and  $\text{OH}_{\text{ad}}$ , the pure double layer capacitance, and pseudo-capacitances of chemisorption are shown in Figure 8 (b)-(d), respectively. The correspondence between line colors and ionic concentrations indicated in Figure 8 (a) is retained in all subfigures. As for the pure double-layer capacitance  $C_{\text{dl}}$  in Figure 8 (c), a Gouy-Chapman minimum is found at  $0.53 \text{ V}_{\text{RHE}}$ . The asymmetry around the pzc is caused by water adsorption. As shown in *Figure 5* (a), a negative value of  $\delta\tilde{\mu}$ , namely, the O-down configuration is more favorable, results in a more tilted increase in  $C_{\text{dl}}$  when the electrode potential moves away from the pzc in the more negative direction. The valley and the terrace of the measured  $C_{\text{total}}$  shifts to lower potentials with increasing concentration of  $\text{LiClO}_4$ . In the present model, the shift in the capacitance minimum and terrace is associated with adsorption of OH, as shown in Figure 8 (d). Possible reasons for this are about to discuss in the next section.

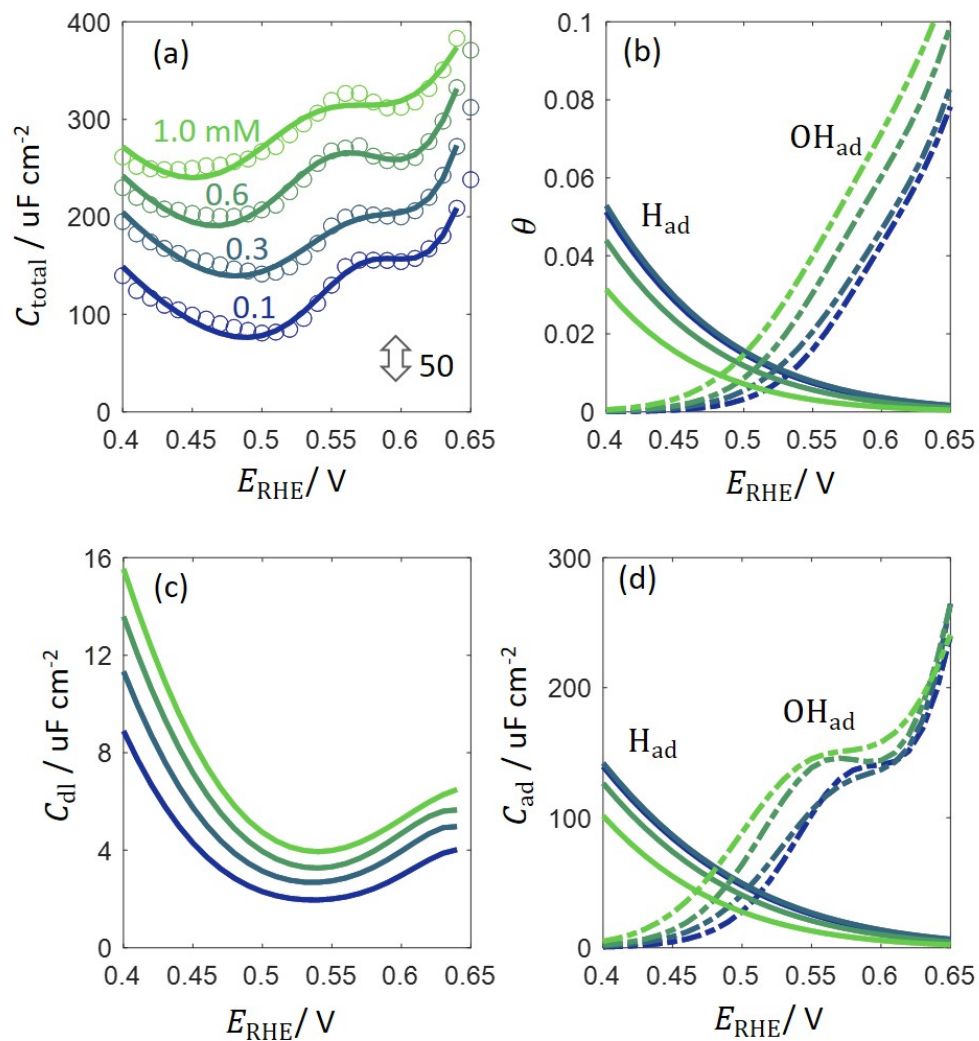


Figure 8 (a) Model-experiment comparison in the presence of different concentrations of LiClO<sub>4</sub> for the electric double layer at Pt(111) in 0.1 mM HClO<sub>4</sub> + x mM LiClO<sub>4</sub>.<sup>22</sup> Model results are marked as solid lines, and experimental data circles. For the sake of clarity, a vertical shift of 50 between different lines is used in (a). The coverages of adsorbed  $\text{H}_{\text{ad}}$  and  $\text{OH}_{\text{ad}}$ , the pure double-layer capacitance,  $C_{\text{dl}}$ , and adsorption capacitances  $C_{\text{H}_{\text{ad}}}$  and  $C_{\text{O}_{\text{H}_{\text{ad}}}}$  are shown in (b), (c) and (d), respectively. Matlab script of this figure is provided in the supporting material of this paper.

## Discussion

### Is there a pure double layer region at Pt(111)?

In contrast with previous works,<sup>22, 51, 52</sup> the present model maintains that voltammogram-derived capacitance of Pt(111) is majorly contributed by  $C_{\text{H}_{\text{ad}}}$  and  $C_{\text{O}_{\text{H}_{\text{ad}}}}$  from a few percentage of active sites,

Figure 8. One of the implications of this claim is that there is no pure double-layer region for the Pt(111) electrode.

The occurrence of chemisorbed  $\text{OH}_{\text{ad}}$  in the so-called double layer potential region could have two causes. On the one hand, there may be structural defects occupying a few percentage of the solid surface.<sup>105, 106</sup> Adsorption of OH (H) occurs at lower (higher) potentials at these structural defects. In a study by Gómez-Marín and Feliu,<sup>107</sup> they experimentally investigated the relation between oxygen reduction activity and step density, and extrapolated this relation to obtain the oxygen reduction activity of an ideally defect-free Pt(111). They found that the extrapolated activity of this ideal Pt(111) is lower than that of a real Pt(111). This comparison leads them to conclude that “This is true even for those electrodes that do not apparently show any step contribution signal in the blank voltammogram, pointing out that a real electrode has always surface defects.” Recent works on stepped Pt electrodes, such as Pt(553)<sup>108</sup> and Pt(311)<sup>109</sup>, have shown low-potential water dissociation in the hydrogen adsorption/desorption region, and the onset potential moves toward the “double layer” region at higher pHs.

On the other hand, interfacial water molecules have an energy distribution, as seen in AIMD simulations.<sup>110</sup> Higher-energy water molecules are decomposed and then adsorbed as  $\text{OH}_{\text{ad}}$  at lower potentials. In general, the electrochemical potentials of protons, water molecules, and adsorbed species at the metal interface are distributed, resulting in a distribution in equilibrium potentials of any electrochemical reaction involving these species. Such a distribution, intrinsically stochastic to a certain extent, echoes the experimental uncertainties found in three repeated measurements on the Pt(111)-0.1 mM  $\text{HClO}_4$  interface. Model results in Figure 8 further indicate that a higher concentration of  $\text{LiClO}_4$  promotes earlier adsorption of OH.

Berna, Climent and Feliu have adopted a similar idea to interpret chemisorption of OH at Pt(111).<sup>111</sup> Specifically, they attributed the broad peak in the low potential region and the sharp peak in the high potential region to the dissociation of two kinds of water molecules with different electrochemical potentials. Their treatment could be regarded as a special case of this model where the distribution function is actually composed of two delta functions.

Currently, it is hard to detect adsorbed intermediates at such a low coverage. Nevertheless, Kondo et al. deduced from their in-situ surface X-ray scattering data that a small amount of oxygen-containing species (unspecified) and/or  $\text{ClO}_4^-$  are adsorbed on Pt(111) immersed in 0.1 M  $\text{HClO}_4$  at 0.57  $V_{\text{RHE}}$  within the double-layer region.<sup>112</sup> It has also been shown that the  $\text{ClO}_4^-$  concentration impacts the CV of Pt(111) in the double layer region.<sup>112, 113</sup> Though I have assumed  $\text{H}_{\text{ad}}$  and  $\text{OH}_{\text{ad}}$  as the chemisorbates when explaining

the experimental data of Ojha et al., the existence of other chemisorbates such as  $\text{ClO}_4^-$  and organic impurities cannot be excluded for this moment.<sup>112, 113</sup>

### **Limitations and possible extensions of the model**

The present double layer model belongs to GCS-type models. An essential feature of these models is the decomposition of the double layer into several subregions which are then described as dielectric continua. The author is aware of harsh criticisms on such GCS-type models regarding drastic simplifications of the double layer structure and its parameterization procedure that arbitrariness slips in.<sup>114</sup> Nevertheless, it is undeniable that GCS-type models are simple yet effective in describing physicochemical properties of the double layer; it forms a valid framework of understanding to interpret atomistic simulations. In addition, I have shown in the model parameterization section how this model can be connected with atomistic simulations.

Though the model results are obtained for a Pt(111) electrode in  $\text{HClO}_4$ -based solution, I do not see principal difficulties in applying it to the alkaline regime, to other electrolyte solution with specifically adsorbing anions such as sulphate and halide ions, and to stepped Pt electrodes. In these new scenarios, the model needs to be extended by including new specific adsorption and/or chemisorption processes, and to be re-parameterized on a case-by-case basis.

The model can be improved on several points: (1) relaxation of the locations of chemisorbed ions and the first water layer as a function of electrode potential; (2) electronic effects of chemisorbed ions and water molecules on  $\chi_M$ ; (3) potential-dependent change of  $\delta\tilde{\mu}$  describing chemical water interactions due to interactions between chemisorbed ions and water molecules; (4) non-covalent interactions between chemisorbed ions and electrolyte species; (5) other chemisorption processes, including those of electrolyte anions and organic impurities, at different types of active sites.

### **Conclusion**

A modified double layer model has been formulated for metal-aqueous interfaces in electrocatalytic systems. The present model divides the inner Helmholtz plane (IHP) further into an AIP (adsorbed ion plane) and ASP (adsorbed solvent plane), accounting for different locations of chemisorbed ions and solvent molecules. The present model employs a statistical treatment of the first-layer water molecules with chemical interactions imposed by the metal, and a distributed treatment of chemisorption of electrolyte species.

The model shows the potential of zero charge, pzc for short, depends on metal-water chemical interactions. I introduce  $\delta\mu$  to characterize the chemical interaction energy difference between water dipoles of  $\alpha_w = 0^\circ$  and that of  $\alpha_w = 180^\circ$ , where  $\alpha_w$  is the angle between water dipole direction and the local electric field. It is found that the pzc becomes higher (lower) when  $\delta\mu > 0$  ( $< 0$ ). In addition to a shift in the pzc, the first-layer water molecules also dramatically elevate the double-layer capacitance  $C_{dl}$ . Equivalently, it means that the first-layer water molecules contribute a negative capacitance component in series with other components, which is a known effect. However, the formula derived in this work to describe this effect, Eq.(26), is, to my knowledge, a new contribution. The model also shows chemisorption-induced dipole moment could lead to a new valley of the capacitance curve, and the capacitance in the valley could take negative values.

The model is then employed to interpret recent CV-based capacitance data of Pt(111)-aqueous solution interfaces. The explanation is based on the ansatz that the experimental data are not the pure double-layer capacitance but include pseudo-capacitances of chemisorption of electrolyte species. This ansatz resolves the discrepancy that the CV-based capacitance values are several fold higher than the values obtained using electrochemical impedance spectroscopy. In addition, it constitutes an alternative angle of understanding stochastic uncertainties found in these experiments. The ansatz and the resulting explanation, though being appealing, must be taken with care, as it implies that there is no pure double layer region even for Pt(111), an aspect that is yet to be confirmed.

Before closing, two experiments to confirm this ansatz are sketched here. One can examine the frequency dependence of interfacial capacitance in the double layer region, especially, at the pzc. If it is a pure double-layer capacitance, there should not be any frequency dispersion below the characteristic frequency of EDL capacitance, which is expressed as  $f_{dl} \propto D/\lambda_D^2$  with  $D$  being the diffusion coefficient of electrolyte ions, and  $\lambda_D$  the Debye length, according to an exact analytical solution developed in Ref.<sup>115</sup> With typical values of  $D = 10^{-9} \text{ m}^2\text{s}^{-1}$  and  $\lambda_D = 1\sim 10 \text{ nm}$ ,  $f_{dl}$  has a range of  $10^7\sim 10^9 \text{ Hz}$ . It is thus safe to claim that a pure double-layer capacitance should not depend on frequency below 1 MHz. In other words, shall one observe that the interfacial capacitance decreases with increasing frequency, it is very likely that the interfacial capacitance contains pseudo-capacitance(s). If it is difficult to obtain reliable high-frequency data, another time-domain method that is easier to implement is to measure the current response to a potential step from the pzc by a small amount, say 20 mV. If it is pure double layer charging, the time constant, expressed as  $t_{dl} \propto 10L\lambda_D/D$  with  $L$  the thickness of diffusion layer,<sup>116</sup> has a range of  $1\sim 10 \text{ ms}$  using typical values of  $D = 10^{-9} \text{ m}^2\text{s}^{-1}$ ,  $L = 100 \text{ }\mu\text{m}$ , and  $\lambda_D = 1\sim 10 \text{ nm}$ . In other words, shall one observe a current ramping with a time constant longer than 10 ms, it is very likely that other slower process(es) is (are) involved.

## Acknowledgement

This work is supported by the Alexander von Humboldt Foundation and the Helmholtz Young Investigators Group Leader Programme. I am grateful to Professors Gary Attard, Juan Feliu, Jianbo Zhang, Katharina Doblhoff-Dier, Ms. Lulu Zhang, and Mr. Jinwen Liu for helpful discussions.

## Declaration of interests

The author declares that they have no known competing financial interests or personal relationships that could have appeared to influence the work reported in this paper.

## Data availability

No new experimental data. The scripts used to calculate the model results are available from the author upon request.

## References

1. Steinmann, S. N.; Seh, Z. W., Understanding electrified interfaces. *Nature Reviews Materials* **2021**, 6 (4), 289-291.
2. Sebastián-Pascual, P.; Shao-Horn, Y.; Escudero-Escribano, M., Toward understanding the role of the electric double layer structure and electrolyte effects on well-defined interfaces for electrocatalysis. *Current Opinion in Electrochemistry* **2022**, 32, 100918.
3. Shin, S.-J.; Kim, D. H.; Bae, G.; Ringe, S.; Choi, H.; Lim, H.-K.; Choi, C. H.; Kim, H., On the importance of the electric double layer structure in aqueous electrocatalysis. *Nature Communications* **2022**, 13 (1), 174.
4. Haid, R. W.; Ding, X.; Sarpey, T. K.; Bandarenka, A. S.; Garlyyev, B., Exploration of the electrical double-layer structure: Influence of electrolyte components on the double-layer capacitance and potential of maximum entropy. *Current Opinion in Electrochemistry* **2022**, 32, 100882.
5. Kozawa, A., Effects of anions and cations on oxygen reduction and oxygen evolution reactions on platinum electrodes. *Journal of Electroanalytical Chemistry (1959)* **1964**, 8 (1), 20-39.
6. Strmcnik, D.; Kodama, K.; van der Vliet, D.; Greeley, J.; Stamenkovic, V. R.; Marković, N. M., The role of non-covalent interactions in electrocatalytic fuel-cell reactions on platinum. *Nature Chemistry* **2009**, 1 (6), 466-472.
7. Strmcnik, D.; van der Vliet, D. F.; Chang, K. C.; Komanicky, V.; Kodama, K.; You, H.; Stamenkovic, V. R.; Marković, N. M., Effects of Li<sup>+</sup>, K<sup>+</sup>, and Ba<sup>2+</sup> Cations on the ORR at Model and High Surface Area Pt and Au Surfaces in Alkaline Solutions. *The Journal of Physical Chemistry Letters* **2011**, 2 (21), 2733-2736.
8. Suntivich, J.; Perry, E. E.; Gasteiger, H. A.; Shao-Horn, Y., The Influence of the Cation on the Oxygen Reduction and Evolution Activities of Oxide Surfaces in Alkaline Electrolyte. *Electrocatalysis* **2013**, 4 (1), 49-55.
9. Resasco, J.; Chen, L. D.; Clark, E.; Tsai, C.; Hahn, C.; Jaramillo, T. F.; Chan, K.; Bell, A. T., Promoter Effects of Alkali Metal Cations on the Electrochemical Reduction of Carbon Dioxide. *Journal of the American Chemical Society* **2017**, 139 (32), 11277-11287.

10. Li, M. F.; Liao, L. W.; Yuan, D. F.; Mei, D.; Chen, Y.-X., pH effect on oxygen reduction reaction at Pt(111) electrode. *Electrochimica Acta* **2013**, *110*, 780-789.
11. Briega-Martos, V.; Herrero, E.; Feliu, J. M., Effect of pH and Water Structure on the Oxygen Reduction Reaction on platinum electrodes. *Electrochimica Acta* **2017**, *241*, 497-509.
12. Ledezma-Yanez, I.; Wallace, W. D. Z.; Sebastián-Pascual, P.; Climent, V.; Feliu, J. M.; Koper, M. T. M., Interfacial water reorganization as a pH-dependent descriptor of the hydrogen evolution rate on platinum electrodes. *Nature Energy* **2017**, *2*, 17031.
13. Rao, R. R.; Huang, B.; Katayama, Y.; Hwang, J.; Kawaguchi, T.; Lunger, J. R.; Peng, J.; Zhang, Y.; Morinaga, A.; Zhou, H.; You, H.; Shao-Horn, Y., pH- and Cation-Dependent Water Oxidation on Rutile RuO<sub>2</sub>(110). *The Journal of Physical Chemistry C* **2021**, *125* (15), 8195-8207.
14. Waagele, M. M.; Gunathunge, C. M.; Li, J.; Li, X., How cations affect the electric double layer and the rates and selectivity of electrocatalytic processes. *The Journal of Chemical Physics* **2019**, *151* (16), 160902.
15. Colic, V.; Pohl, M. D.; Scieszka, D.; Bandarenka, A. S., Influence of the electrolyte composition on the activity and selectivity of electrocatalytic centers. *Catalysis Today* **2016**, *262*, 24-35.
16. Moura de Salles Pupo, M.; Kortlever, R., Electrolyte Effects on the Electrochemical Reduction of CO<sub>2</sub>. *ChemPhysChem* **2019**, *20* (22), 2926-2935.
17. Deng, B.; Huang, M.; Zhao, X.; Mou, S.; Dong, F., Interfacial Electrolyte Effects on Electrocatalytic CO<sub>2</sub> Reduction. *ACS Catalysis* **2022**, *12* (1), 331-362.
18. Pajkossy, T.; Kolb, D. M., Double layer capacitance of Pt(111) single crystal electrodes. *Electrochimica Acta* **2001**, *46* (20), 3063-3071.
19. Pajkossy, T., Voltammetry and Impedance of Pt(111) Electrodes in Aqueous KClO<sub>4</sub> Solutions. In *Zeitschrift für Physikalische Chemie*, 2003; Vol. 217, p 351.
20. Pajkossy, T.; Kolb, D. M., On the origin of the double layer capacitance maximum of Pt(111) single crystal electrodes. *Electrochemistry Communications* **2003**, *5* (4), 283-285.
21. Ojha, K.; Arulmozhi, N.; Aranzales, D.; Koper, M. T. M., Double Layer at the Pt(111)–Aqueous Electrolyte Interface: Potential of Zero Charge and Anomalous Gouy–Chapman Screening. *Angewandte Chemie International Edition* **2020**, *59* (2), 711-715.
22. Ojha, K.; Doblhoff-Dier, K.; Koper Marc, T. M., Double-layer structure of the Pt(111)–aqueous electrolyte interface. *Proceedings of the National Academy of Sciences* **2022**, *119* (3), e2116016119.
23. Xue, S.; Garlyyev, B.; Auer, A.; Kunze-Liebhäuser, J.; Bandarenka, A. S., How the Nature of the Alkali Metal Cations Influences the Double-Layer Capacitance of Cu, Au, and Pt Single-Crystal Electrodes. *The Journal of Physical Chemistry C* **2020**, *124* (23), 12442-12447.
24. Schmickler, W.; Santos, E., *Interfacial electrochemistry*. Springer-Verlag Berlin Heidelberg: New York, 2010; p XII, 270.
25. Guidelli, R.; Schmickler, W., Recent developments in models for the interface between a metal and an aqueous solution. *Electrochimica Acta* **2000**, *45* (15), 2317-2338.
26. Damaskin, B. B.; Petrii, O. A., Historical development of theories of the electrochemical double layer. *J. Solid State Electrochem.* **2011**, *15* (7), 1317-1334.
27. Lu-Lu Zhang, C.-K. L. J. H., A Beginners' Guide to Modelling of Electric Double Layer Under Equilibrium, Nonequilibrium and Ac Conditions. *Journal of Electrochemistry* **2021**, *0*.
28. Kornyshev, A. A., Double-Layer in Ionic Liquids: Paradigm Change? *J. Phys. Chem. B* **2007**, *111* (20), 5545-5557.
29. Budkov, Y. A.; Kolesnikov, A. L., Electric double layer theory for room temperature ionic liquids on charged electrodes: Milestones and prospects. *Current Opinion in Electrochemistry* **2022**, *33*, 100931.
30. Gouy, G., Sur La Constitution De La Charge Electrique A La Surface D'Un Electrolyte. *J. Phys. Theor. Appl.* **1910**, *9*, 457-468.
31. Grahame, D. C., The Electrical Double Layer and the Theory of Electrocapillarity. *Chem. Rev.* **1947**, *41* (3), 441-501.
32. Parsons, R., The electrical double layer: recent experimental and theoretical developments. *Chem. Rev.* **1990**, *90* (5), 813-826.



33. Mott, N. F.; Watts-Tobin, R. J., The interface between a metal and an electrolyte. *Electrochimica Acta* **1961**, 4 (2), 79-107.
34. Watts-tobin, R. J., The interface between a metal and an electrolytic solution. *The Philosophical Magazine: A Journal of Theoretical Experimental and Applied Physics* **1961**, 6 (61), 133-153.
35. Macdonald, J. R.; Barlow, C. A., Theory of Double-Layer Differential Capacitance in Electrolytes. *The Journal of Chemical Physics* **1962**, 36 (11), 3062-3080.
36. Bockris, J. O. M.; Habib, M. A., Contributions of water dipoles to double layer properties: A three-state water model. *Electrochimica Acta* **1977**, 22 (1), 41-46.
37. Levine, S.; Bell, G. M.; Calvert, D., THE DISCRETENESS-OF-CHARGE EFFECT IN ELECTRIC DOUBLE LAYER THEORY. *Canadian Journal of Chemistry* **1962**, 40 (3), 518-538.
38. Fawcett, W. R.; Levine, S., Discreteness-of-charge effects in electrode kinetics. *Journal of Electroanalytical Chemistry and Interfacial Electrochemistry* **1973**, 43 (2), 175-184.
39. Grahame, D. C., Discreteness-of-charge-effects in the inner region of the electrical double layer. *Zeitschrift für Elektrochemie, Berichte der Bunsengesellschaft für physikalische Chemie* **1958**, 62 (3), 264-274.
40. Fawcett, W. R., Fifty years of studies of double layer effects in electrode kinetics—a personal view. *Journal of Solid State Electrochemistry* **2011**, 15 (7), 1347.
41. Badiali, J. P.; Rosinberg, M. L.; Goodisman, J., Contribution of the metal to the differential capacity of an ideally polarisable electrode. *J. Electroanal. Chem.* **1983**, 143 (1), 73-88.
42. Badiali, J. P.; Rosinberg, M. L.; Vericat, F.; Blum, L., A microscopic model for the liquid metal-ionic solution interface. *J. Electroanal. Chem.* **1983**, 158 (2), 253-267.
43. Schmickler, W., A jellium-dipole model for the double layer. *J. Electroanal. Chem.* **1983**, 150 (1), 19-24.
44. Kornyshev, A. A., Metal electrons in the double layer theory. *Electrochim. Acta* **1989**, 34 (12), 1829-1847.
45. Valette, G., Double layer on silver single-crystal electrodes in contact with electrolytes having anions which present a slight specific adsorption: Part I. The (110) face. *Journal of Electroanalytical Chemistry and Interfacial Electrochemistry* **1981**, 122, 285-297.
46. Valette, G., Double layer on silver single crystal electrodes in contact with electrolytes having anions which are slightly specifically adsorbed: Part II. The (100) face. *Journal of Electroanalytical Chemistry and Interfacial Electrochemistry* **1982**, 138 (1), 37-54.
47. Valette, G., Double layer on silver single crystal electrodes in contact with electrolytes having anions which are slightly specifically adsorbed: Part III. The (111) face. *Journal of Electroanalytical Chemistry and Interfacial Electrochemistry* **1989**, 269 (1), 191-203.
48. Hamelin, A.; Foresti, M. L.; Guidelli, R., Test of the Gouy-Chapman theory at a (111) silver single-crystal electrode. *Journal of Electroanalytical Chemistry* **1993**, 346 (1), 251-259.
49. Pajkossy, T.; Kolb, D. M., Double layer capacitance of the platinum group metals in the double layer region. *Electrochemistry Communications* **2007**, 9 (5), 1171-1174.
50. Schouten, K. J. P.; van der Niet, M. J. T. C.; Koper, M. T. M., Impedance spectroscopy of H and OH adsorption on stepped single-crystal platinum electrodes in alkaline and acidic media. *Physical Chemistry Chemical Physics* **2010**, 12 (46), 15217-15224.
51. Doblhoff-Dier, K.; Koper, M. T. M., Modeling the Gouy–Chapman Diffuse Capacitance with Attractive Ion–Surface Interaction. *The Journal of Physical Chemistry C* **2021**, 125 (30), 16664-16673.
52. Schmickler, W., The Effect of Weak Adsorption on the Double Layer Capacitance. *ChemElectroChem* **2021**, 8 (22), 4218-4222.
53. Le, J.-B.; Fan, Q.-Y.; Li, J.-Q.; Cheng, J., Molecular origin of negative component of Helmholtz capacitance at electrified Pt(111)/water interface. *Science Advances* **2021**, 6 (41), eabb1219.
54. Sibert, E.; Faure, R.; Durand, R., High frequency impedance measurements on Pt(111) in sulphuric and perchloric acids. *Journal of Electroanalytical Chemistry* **2001**, 515 (1), 71-81.

55. Grahame, D. C., Components of Charge and Potential in the Non-diffuse Region of the Electrical Double Layer: Potassium Iodide Solutions in Contact with Mercury at 25°1. *Journal of the American Chemical Society* **1958**, *80* (16), 4201-4210.
56. Grahame, D. C.; Parsons, R., Components of Charge and Potential in the Inner Region of the Electrical Double Layer: Aqueous Potassium Chloride Solutions in Contact with Mercury at 25°. *Journal of the American Chemical Society* **1961**, *83* (6), 1291-1296.
57. Grahame, D. C., The Electrical Double Layer and the Theory of Electrocapillarity. *Chemical Reviews* **1947**, *41* (3), 441-501.
58. Damaskin, B.; Pankratova, I.; Palm, U.; Anni, K.; Väärtnõu, M.; Salve, M., Comparison of the ionic adsorption theories for the electrode/solution interface by computer simulation. *Journal of Electroanalytical Chemistry and Interfacial Electrochemistry* **1987**, *234* (1), 31-53.
59. Kolotyrkin, Y. M.; Alexeyev, Y. V.; Popov, Y. A., Double layer model taking into account the specific adsorption of ions: Application to the process of hydrogen adsorption on lead in the presence of iodide ion. *Journal of Electroanalytical Chemistry and Interfacial Electrochemistry* **1975**, *62* (1), 135-149.
60. Vorotyntsev, M., Chemisorption theory for charged species at electrodes in the model of an energetically homogeneous surface. *Journal of The Research Institute for Catalysis Hokkaido University* **1983**, *30* (3), 167-177.
61. Guidelli, R., Monolayer Models of Metal-Water Interphases and their use in the Interpretation of Differential Capacity Curves and of Organic Adsorption. In *Trends in Interfacial Electrochemistry*, Silva, A. F., Ed. Springer Netherlands: Dordrecht, 1986; pp 387-452.
62. Trasatti, S., Work function, electronegativity, and electrochemical behaviour of metals: II. Potentials of zero charge and “electrochemical” work functions. *Journal of Electroanalytical Chemistry and Interfacial Electrochemistry* **1971**, *33* (2), 351-378.
63. Damaskin, B. B.; Frumkin, A. N., Potentials of zero charge, interaction of metals with water and adsorption of organic substances—III. The role of the water dipoles in the structure of the dense part of the electric double layer. *Electrochimica Acta* **1974**, *19* (4), 173-176.
64. Bockris, J. O. M.; Devanathan, M. A. V.; Müller, K., On the structure of charged interfaces. *Proc. Roy. Soc. A* **1963**, *274* (1356), 55-79.
65. Sakong, S.; Forster-Tonigold, K.; Groß, A., The structure of water at a Pt(111) electrode and the potential of zero charge studied from first principles. *J. Chem. Phys.* **2016**, *144* (19), 194701.
66. Le, J.; Iannuzzi, M.; Cuesta, A.; Cheng, J., Determining Potentials of Zero Charge of Metal Electrodes versus the Standard Hydrogen Electrode from Density-Functional-Theory-Based Molecular Dynamics. *Phys. Rev. Lett.* **2017**, *119* (1), 016801.
67. Sakong, S.; Groß, A., The electric double layer at metal-water interfaces revisited based on a charge polarization scheme. *J. Chem. Phys.* **2018**, *149* (8), 084705.
68. Le, J.-B.; Chen, A.; Li, L.; Xiong, J.-F.; Lan, J.; Liu, Y.-P.; Iannuzzi, M.; Cheng, J., Modeling Electrified Pt(111)-Had/Water Interfaces from Ab Initio Molecular Dynamics. *JACS Au* **2021**.
69. Groß, A.; Sakong, S., Ab Initio Simulations of Water/Metal Interfaces. *Chemical Reviews* **2022**.
70. Schmickler, W.; Guidelli, R., The partial charge transfer. *Electrochim. Acta* **2014**, *127*, 489-505.
71. Carnie, S. L.; Chan, D. Y. C., The modelling of solvent structure in the electrical double layer. *Advances in Colloid and Interface Science* **1982**, *16* (1), 81-100.
72. Schmickler, W.; Guidelli, R., Ionic adsorption and the surface dipole potential. *Journal of Electroanalytical Chemistry and Interfacial Electrochemistry* **1987**, *235* (1), 387-392.
73. Huang, J.; Malek, A.; Zhang, J.; Eikerling, M. H., Non-monotonic Surface Charging Behavior of Platinum: A Paradigm Change. *The Journal of Physical Chemistry C* **2016**, *120* (25), 13587-13595.
74. Huang, J.; Zhou, T.; Zhang, J.; Eikerling, M., Double layer of platinum electrodes: Non-monotonic surface charging phenomena and negative double layer capacitance. *The Journal of Chemical Physics* **2018**, *148* (4), 044704.
75. Zhang, M.-K.; Cai, J.; Chen, Y.-X., On the electrode charge at the metal/solution interface with specific adsorption. *Current Opinion in Electrochemistry* **2022**, *36*, 101161.

76. Frumkin, A. N.; Petrii, O. A., Potentials of zero total and zero free charge of platinum group metals. *Electrochimica Acta* **1975**, 20 (5), 347-359.
77. Damaskin, B. B.; Safonov, V. A.; Petrii, O. A., Model of two limiting states for describing the properties of the electric double layer in the absence of specific adsorption of ions. *Journal of Electroanalytical Chemistry and Interfacial Electrochemistry* **1989**, 258 (1), 13-25.
78. Safonov, V. A.; Krivenko, A. G.; Choba, M. A., Initial oxidation of silver electrode in weakly acidic sodium fluoride solutions: Potential shifts induced by laser heating. *Electrochimica Acta* **2008**, 53 (14), 4859-4866.
79. Garcia-Araez, N.; Climent, V.; Feliu, J., Potential-Dependent Water Orientation on Pt(111), Pt(100), and Pt(110), As Inferred from Laser-Pulsed Experiments. Electrostatic and Chemical Effects. *The Journal of Physical Chemistry C* **2009**, 113 (21), 9290-9304.
80. Sarabia, F. J.; Sebastián, P.; Climent, V.; Feliu, J. M., New insights into the Pt(hkl)-alkaline solution interphases from the laser induced temperature jump method. *Journal of Electroanalytical Chemistry* **2020**, 872, 114068.
81. Huang, J., Surface charging behaviors of electrocatalytic interfaces with partially charged chemisorbates. *Current Opinion in Electrochemistry* **2022**, 33, 100938.
82. Gongadze, E.; Iglič, A., Decrease of permittivity of an electrolyte solution near a charged surface due to saturation and excluded volume effects. *Bioelectrochemistry* **2012**, 87, 199-203.
83. Levy, A.; Andelman, D.; Orland, H., Dipolar Poisson-Boltzmann approach to ionic solutions: A mean field and loop expansion analysis. *The Journal of Chemical Physics* **2013**, 139 (16), 164909.
84. Braunwarth, L.; Jung, C.; Jacob, T., Potential-Dependent Pt(111)/Water Interface: Tackling the Challenge of a Consistent Treatment of Electrochemical Interfaces\*\*. *ChemPhysChem* **2022**, n/a (n/a), e202200336.
85. Kastlunger, G.; Lindgren, P.; Peterson, A. A., Controlled-Potential Simulation of Elementary Electrochemical Reactions: Proton Discharge on Metal Surfaces. *The Journal of Physical Chemistry C* **2018**, 122 (24), 12771-12781.
86. Foresti, M. L.; Innocenti, M.; Forni, F.; Guidelli, R., Electrosorption Valency and Partial Charge Transfer in Halide and Sulfide Adsorption on Ag(111). *Langmuir* **1998**, 14 (24), 7008-7016.
87. Zhang, Y.; Huang, J., Treatment of Ion-Size Asymmetry in Lattice-Gas Models for Electrical Double Layer. *J. Phys. Chem. C* **2018**, 122 (50), 28652-28664.
88. Qing, L.; Jiang, J., Double-Edged Sword of Ion-Size Asymmetry in Energy Storage of Supercapacitors. *The Journal of Physical Chemistry Letters* **2022**, 13 (6), 1438-1445.
89. Bossa, G. V.; Caetano, D. L. Z.; de Carvalho, S. J.; May, S., Differential capacitance of an electrical double layer with asymmetric ion sizes in the presence of hydration interactions. *Electrochimica Acta* **2019**, 321, 134655.
90. Gongadze, E.; Iglič, A., Asymmetric size of ions and orientational ordering of water dipoles in electric double layer model - an analytical mean-field approach. *Electrochimica Acta* **2015**, 178, 541-545.
91. Garcia-Araez, N.; Climent, V.; Feliu, J. M., Analysis of temperature effects on hydrogen and OH adsorption on Pt(111), Pt(100) and Pt(110) by means of Gibbs thermodynamics. *Journal of Electroanalytical Chemistry* **2010**, 649 (1), 69-82.
92. Climent, V.; Gómez, R.; Orts, J. M.; Feliu, J. M., Thermodynamic Analysis of the Temperature Dependence of OH Adsorption on Pt(111) and Pt(100) Electrodes in Acidic Media in the Absence of Specific Anion Adsorption. *The Journal of Physical Chemistry B* **2006**, 110 (23), 11344-11351.
93. Hörmann, N. G.; Reuter, K., Thermodynamic cyclic voltammograms: peak positions and shapes. *Journal of Physics: Condensed Matter* **2021**, 33 (26), 264004.
94. Huang, J., Hybrid density-potential functional theory of electric double layers. *Electrochimica Acta* **2021**, 389, 138720.
95. Trasatti, S., The “absolute” electrode potential—the end of the story. *Electrochimica Acta* **1990**, 35 (1), 269-271.
96. Melander, M.; Wu, T.; Honkala, K., Constant inner potential DFT for modelling electrochemical systems under constant potential and bias. **2021**, 10.26434/chemrxiv-2021-r621x-v2.

97. Putintsev, N. M.; Putintsev, D. N., High-frequency dielectric permittivity of water and its components. *Russian Journal of Physical Chemistry A* **2011**, 85 (7), 1113-1118.
98. Bockris, J. O. m.; Devanathan, M. A. V.; Müller, K.; Butler, J. A. V., On the structure of charged interfaces. *Proceedings of the Royal Society of London. Series A. Mathematical and Physical Sciences* **1963**, 274 (1356), 55-79.
99. Schnur, S.; Groß, A., Properties of metal–water interfaces studied from first principles. *New Journal of Physics* **2009**, 11 (12), 125003.
100. Sakong, S.; Groß, A., Water structures on a Pt(111) electrode from ab initio molecular dynamic simulations for a variety of electrochemical conditions. *Phys. Chem. Chem. Phys.* **2020**, 22 (19), 10431-10437.
101. Abrashkin, A.; Andelman, D.; Orland, H., Dipolar Poisson-Boltzmann Equation: Ions and Dipoles Close to Charge Interfaces. *Physical Review Letters* **2007**, 99 (7), 077801.
102. Malek, A.; Eikerling, M. H., Chemisorbed Oxygen at Pt(111): a DFT Study of Structural and Electronic Surface Properties. *Electrocatalysis* **2018**, 9 (3), 370-379.
103. Martínez-Hincapié, R.; Sebastián-Pascual, P.; Climent, V.; Feliu, J. M., Exploring the interfacial neutral pH region of Pt(111) electrodes. *Electrochemistry Communications* **2015**, 58, 62-64.
104. Kobayashi, K.; Suzuki, T. S., Distribution of Relaxation Time Analysis for Non-ideal Immittance Spectrum: Discussion and Progress. *Journal of the Physical Society of Japan* **2018**, 87 (9), 094002.
105. Fernández, P. S.; Tereshchuk, P.; Angelucci, C. A.; Gomes, J. F.; Garcia, A. C.; Martins, C. A.; Camara, G. A.; Martins, M. E.; Da Silva, J. L. F.; Tremiliosi-Filho, G., How do random superficial defects influence the electro-oxidation of glycerol on Pt(111) surfaces? *Physical Chemistry Chemical Physics* **2016**, 18 (36), 25582-25591.
106. Nie, S.; Feibelman, P. J.; Bartelt, N. C.; Thürmer, K., Pentagons and Heptagons in the First Water Layer on Pt(111). *Physical Review Letters* **2010**, 105 (2), 026102.
107. Gómez-Marín, A. M.; Feliu, J. M., Oxygen reduction on nanostructured platinum surfaces in acidic media: Promoting effect of surface steps and ideal response of Pt(111). *Catalysis Today* **2015**, 244, 172-176.
108. Chen, X.; McCrum, I. T.; Schwarz, K. A.; Janik, M. J.; Koper, M. T. M., Co-adsorption of Cations as the Cause of the Apparent pH Dependence of Hydrogen Adsorption on a Stepped Platinum Single-Crystal Electrode. *Angewandte Chemie International Edition* **2017**, 56 (47), 15025-15029.
109. Rizo, R.; Fernández-Vidal, J.; Hardwick, L. J.; Attard, G. A.; Vidal-Iglesias, F. J.; Climent, V.; Herrero, E.; Feliu, J. M., Investigating the presence of adsorbed species on Pt steps at low potentials. *Nature Communications* **2022**, 13 (1), 2550.
110. Korpelin, V.; Kiljunen, T.; Melander, M. M.; Caro, M. A.; Kristoffersen, H. H.; Mammen, N.; Apaja, V.; Honkala, K., Addressing Dynamics at Catalytic Heterogeneous Interfaces with DFT-MD: Anomalous Temperature Distributions from Commonly Used Thermostats. *The Journal of Physical Chemistry Letters* **2022**, 13 (11), 2644-2652.
111. Berná, A.; Climent, V.; Feliu, J. M., New understanding of the nature of OH adsorption on Pt(111) electrodes. *Electrochemistry Communications* **2007**, 9 (12), 2789-2794.
112. Kondo, T.; Masuda, T.; Aoki, N.; Uosaki, K., Potential-Dependent Structures and Potential-Induced Structure Changes at Pt(111) Single-Crystal Electrode/Sulfuric and Perchloric Acid Interfaces in the Potential Region between Hydrogen Underpotential Deposition and Surface Oxide Formation by In Situ Surface X-ray Scattering. *The Journal of Physical Chemistry C* **2016**, 120 (29), 16118-16131.
113. Attard, G. A.; Brew, A.; Hunter, K.; Sharman, J.; Wright, E., Specific adsorption of perchlorate anions on Pt{hkl} single crystal electrodes. *Physical Chemistry Chemical Physics* **2014**, 16 (27), 13689-13698.
114. Schmickler, W., Double layer theory. *Journal of Solid State Electrochemistry* **2020**, 24 (9), 2175-2176.
115. Li, C. K.; Huang, J., Impedance Response of Electrochemical Interfaces: Part I. Exact Analytical Expressions for Ideally Polarizable Electrodes. *Journal of The Electrochemical Society* **2021**, 167 (16), 166517.

116. Huang, J., On obtaining double-layer capacitance and potential of zero charge from voltammetry. *Journal of Electroanalytical Chemistry* **2020**, 870, 114243.